Microscopic description of the shape coexistence in the $A \sim 70$ mass region

A. Petrovici,[1,2,3)] K. W. Schmid,[2)] and A. Faessler[2)]

Fiz. Elem. Chastits At. Yadra **23**, 914–973 (July–August 1992)

The shape-coexistence phenomena dominating the structure of the nuclei in the $A \sim 70$ mass region are investigated within different approaches using general symmetry-projected Hartree–Fock–Bogolyubov configurations as basic building blocks, a rather large model space, and a suitably defined effective two-body interaction. The selection of the relevant configurations determines the dynamics of the considered system in the framework of the EXCITED VAMPIR and EXCITED FED VAMPIR variational procedures involving *real* or *complex* mean fields. The results concerning the structure of low- and high-spin states in a number of even–even Ge, Se, and Kr nuclei indicate that a variable mixing of more or less deformed prolate and oblate quasiparticle determinants is responsible for the complex behavior of the doubly even nuclei in this mass region.

1. INTRODUCTION

Studies of nuclei far from stability revealed an unexpected variety of nuclear structures and motions which are challenging and continuously improving our understanding of a nucleus. The experimental investigations progressed with the development of acceleration techniques, improvement of isotope separation, advances in instrumentation, and new detection methods. On the other hand, the new experimental information concerning low- and high-spin spectra, electromagnetic properties of short-lived states, and also inelastic electron scattering data gave a challenge to theoretical nuclear-structure physics and led to a rapid development of rather successful theoretical methods.

Particular attention has been paid to the nuclei belonging to the $A \sim 70$ mass region. According to both the experimental systematics and the theoretical calculations, the mass $A \sim 70$ nuclei have a transitional character and display a rich pattern of shape coexistence and shape transition. The multiplicity of structures, the rapid and also drastic changes of the properties with the number of nucleons, and the interplay of collective and single-particle motions make the $A = 70$–80 region an important testing ground for nuclear models.[1] Unfortunately, a microscopic insight into the shape-coexistence phenomena dominating the structure of the mass-70 region by a complete diagonalization of a suitably chosen effective many-nucleon Hamiltonian, as is done in the Shell-Model Configuration Mixing (SCM) approach, is severely hindered, because a large number of valence nucleons are distributed among many single-particle levels. Therefore the theoretical studies[2–11] which tried to explain the interesting behavior of doubly even nuclei around mass number $A \sim 70$ have been carried out either in rather restricted configuration spaces in the framework of the usual shell model or by using several collective models or models involving an interplay of particles and collective excitations. A clear understanding of all the known facts was not possible.

The even–even nuclei of the $A \sim 70$ region display a number of interesting features which are rather unique in the nuclear mass table (see, e.g., Ref. 1 and references therein). The coexistence of overlapping bands built on different nuclear shapes, and also the observation of many low-spin states, e.g., 0^+ or 2^+ states, at very low excitation energy, is related to the competition between various large gaps at different deformations displayed by the Nilsson single-particle energy diagrams. Furthermore, the nuclei in this mass region usually have both active protons and neutrons in the $0g_{9/2}$ shell-model orbit. Since there are many different ways to couple these particles to intermediate and high-spin values, a competition of many configurations at these spin values is also rather likely.

For a deeper theoretical understanding of the complex experimental situation encountered in the mass $A \sim 70$ nuclei, one needs a microscopic model in which all the essential degrees of freedom of collective as well as single-particle nature are not put in by hand but are included in a completely microscopic fashion. For this purpose we use here the variational techniques developed for various models of the so-called VAMPIR (Variation After Mean Field Projection In Realistic model spaces) family.[12] The two most sophisticated procedures in this family, which has been continuously extended and improved during the last couple of years, are the EXCITED VAMPIR and EXCITED FED VAMPIR approximations. As we shall see, these are rather adequate to describe the shape-coexistence phenomena.

The EXCITED VAMPIR model is essentially a mean-field theory which solves the Hartree–Fock–Bogolyubov problem with spin and number projection before the variation for yrast and nonyrast states. In this approximation an optimized mean field is obtained for each state of a given symmetry by a chain of independent variational calculations and, finally, the residual interaction in the resulting A-nucleon configuration space is diagonalized. Our first investigations concerned the low-spin excitation spectra for a number of doubly even Ge as well as Se isotopes[13] in the framework of the EXCITED VAMPIR model based on *real* HFB transformations. We found that a variable mixing of more or less deformed prolate and oblate projected

 0090-4759/92/040402-28$04.00 © 1993 American Institute of Physics

quasiparticle determinants is able to produce the experimental picture for the low-spin states of the considered Ge and Se isotopes, like the presence of 4–5 coexisting 0^+ or 2^+ states below 3–4 MeV excitation energy, as well as the general trends in the quadrupole moments, the $B(E0)$ and $B(E2)$ values, and the proton and neutron occupations of the spherical single-particle orbitals. These results strongly supported the shape coexistence as a dominant feature of the low-spin states in even Ge and Se nuclei.

Encouraged by this success, the *real* EXCITED VAMPIR investigations were extended to the high-spin states in the ^{68}Ge, ^{70}Se, and ^{72}Se nuclei.[14] It turned out that the shape coexistence persists and manifests itself specifically at high-spin states. A strong bunching of states of a given spin and parity in a small excitation-energy interval was predicted, as well as a variable, sometimes very strong, mixing between these states which creates a complex feeding pattern for the yrast band, including competing $M1$, $\Delta I=0$ transitions. Nevertheless, the high-spin states could still be grouped into bands based on different structures, some of them connected by $E2$ crossing transitions.

In order to understand how reliable the EXCITED VAMPIR description of the considered states really was, an improvement of the theoretical approximation was necessary. This was achieved by the so-called EXCITED FED (from FEw Determinants) VAMPIR method,[15,16] which goes beyond the symmetry-projected quasiparticle mean-field approximation. In this approach each state is described not by only one determinant, but by a linear combination of a few projected determinants obtained successively in a chain of variational calculations, asking in each step for maximum residual interaction and thus for a maximum additional contribution to that state. By this procedure the remaining residual interaction between the resulting few lowest states of a given symmetry becomes much smaller than in the case of the uncorrelated EXCITED VAMPIR solutions, and thus the reliability of the wave functions is increased considerably. The nature of each high-spin band is more precisely distinguished, since the dominant correlations for each particular configuration are included in a systematic way. Reinvestigating the low- and high-spin states of ^{68}Ge with this new method, we found that the qualitative features of the EXCITED VAMPIR description persist. It was also possible to identify, from among the many overlapping bands, one having considerably larger deformation, $\beta_2\sim 0.42$, than the other bands in ^{68}Ge and in other Ge nuclei. This is a strikingly large deformation for such a light nucleus; however, as we shall see, recent experimental data confirm this prediction.[17]

A more quantitative confirmation of the rather complicated theoretical picture of the structure of the nuclei in the $A\sim 70$ mass region comes from the comparison of the charge and transition charge densities in several even Ge isotopes[18] with the available data extracted from elastic and inelastic electron scattering.[19]

Quantitative changes of the complex picture emerging from these studies which are only based on *real* Hartree–Fock–Bogolyubov transformations had to be expected when we included unnatural-parity pairing correlations by essentially *complex* mean fields. However, the qualitative features of the complex behavior of the nuclei in this mass region persist even in such more refined calculations, as indicated by the first results which we obtained very recently within the *complex* versions of the VAMPIR models.[23]

In this review only selected highlights will be presented, which will include: the basic ideas behind the microscopic approaches used in our theoretical investigations; the *real* EXCITED VAMPIR picture concerning the coexistence of multiple shapes and structures associated with quite different deformations in a number of even Ge and Se isotopes at low excitations; some new aspects of the nuclear shape coexistence in the $A\sim 70$ mass region obtained by going beyond symmetry-projected quasiparticle mean fields; new insights into the structure of $N=Z$ nuclei gained by using complex mean fields. These new results may illustrate the power of the continuously developing realistic microscopic approaches belonging to the VAMPIR model family.

2. THE THEORETICAL FRAMEWORK

In this section we shall briefly sketch the EXCITED VAMPIR and EXCITED FED VAMPIR approximations, the most sophisticated variational procedures of the VAMPIR model family, where the construction of the configuration space itself is left entirely to the dynamics of the considered system and determined by a chain of successive variational calculations. Also, we shall discuss the basic assumptions and ingredients of the models as well as the model space and the effective interaction.

2.1. Basic assumptions and ingredients of the theory

We restrict ourselves to the investigation of the structure of the nuclear ground state and low-lying discrete excitations at "low excitation energy and momentum transfer." Therefore we assume that it is possible to use an effective two-body interaction in a finite model space. The effective many-nucleon Hamiltonian appropriate for a finite model space in a given mass region consisting of general one- and two-body terms is assumed to be given by

$$\hat{H}=\sum_{i,k=1}^{M} t(ik)c_i^\dagger c_k+\frac{1}{4}\sum_{i,k,r,s=1}^{M} v(ikrs)c_i^\dagger c_k^\dagger c_s c_r\,, \qquad (2.1)$$

where $t(ik)\equiv\langle i|\hat{t}|k\rangle$ are the matrix elements of the one-body operator of the kinetic energy (or, if an inert core is used, some suitably chosen single-particle energies) and $v(ikrs)\equiv\langle ik|\hat{v}|rs-sr\rangle$ are the antisymmetrized matrix elements of the effective two-body interaction. The Hamiltonian is represented in terms of creation $\{c_i^\dagger,c_k^\dagger,\ldots\}_M$ and annihilation $\{c_i,c_k,\ldots\}_M$ fermion operators corresponding to our model space defined by a finite, M-dimensional set $\{|i\rangle,|k\rangle,\ldots\}_M$ of orthonormal single-nucleon states, e.g., harmonic-oscillator wave functions.

The truncation schemes which we use to get the best approximations to the (in large model spaces) inaccessible

"exact" solutions are based on the Hartree–Fock–Bogolyubov (HFB) theory.

The first step to the ansatz of our many-body wave function is to define the quasiparticle creators and annihilators via

$$a_\alpha^\dagger \equiv \sum_{i=1}^{M} (A_{i\alpha} c_i^\dagger + B_{i\alpha} c_i), \tag{2.2}$$

$$a_\alpha \equiv \sum_{i=1}^{M} (B_{i\alpha}^* c_i^\dagger + A_{i\alpha}^* c_i). \tag{2.3}$$

In matrix notation these equations can be combined to

$$\begin{pmatrix} a^\dagger \\ a \end{pmatrix} = \begin{pmatrix} A^T & B^T \\ B^\dagger & A^\dagger \end{pmatrix} \begin{pmatrix} c^\dagger \\ c \end{pmatrix} \equiv F \begin{pmatrix} c^\dagger \\ c \end{pmatrix} \tag{2.4}$$

where F is a unitary $(2M \times 2M)$-dimensional matrix.

The corresponding HFB vacuum is defined by $a_\alpha |F\rangle \equiv 0$ for all $\alpha = 1,...,M$ and can be represented as

$$|F\rangle = \left(\prod_{\alpha=1}^{M'} a_\alpha \right) |0\rangle \quad \text{with } M' \leqslant M. \tag{2.5}$$

Since the transformation (2.4) sums over all the quantum numbers characterizing the single-particle basis states, $|F\rangle$ violates angular momentum, particle number, and charge conservation and, in general, has no definite parity either. In order to obtain the physical configurations, we have to restore the broken symmetries.

From the vacuum (2.5) configurations with the desired symmetry quantum numbers $s \equiv A T_z I^\pi$ can be constructed using the operator

$$\hat{\Theta}_{MK}^s \equiv \hat{P}(IM;K) \hat{Q}(2T_z) \hat{Q}(A) \hat{p}(\pi). \tag{2.6}$$

Here

$$\hat{p}(\pi) \equiv \tfrac{1}{2}(1 + \pi \hat{\Pi}), \tag{2.7}$$

where $\hat{\Pi}$ is the parity operator, projects onto definite parity π;

$$\hat{Q}(A) \equiv \frac{1}{2\pi} \int_0^{2\pi} d\varphi \exp\{i\varphi(A - \hat{A})\}, \tag{2.8}$$

where $\hat{A}$ is the nucleon-number operator, restores the desired total nucleon number A; and

$$\hat{Q}(2T_z) \equiv \frac{1}{2\pi} \int_0^{2\pi} d\chi \exp\{i\chi(N - Z - \hat{N} + \hat{Z})\}, \tag{2.9}$$

where $\hat{N}$ and $\hat{Z}$ are the neutron- and proton-number operators, respectively, selects the components with a definite total isospin projection $2T_z = N - Z$. Finally,

$$\hat{P}(IM;K) \equiv \frac{2I+1}{8\pi^2} \int_0^{4\pi} d\Omega D_{MK}^I(\Omega) \hat{R}(\Omega), \tag{2.10}$$

where $\hat{R}(\Omega)$ is the usual rotation operator and $D_{MK}^I(\Omega)$ denotes its representation in angular-momentum eigenstates, constructs from the $I_3 = K$ component in the symmetry-breaking "intrinsic" frame of reference a configuration in the laboratory frame with total angular momentum I and 3-component $I_z = M$. The unphysical dependence on the orientation of the intrinsic quantization axis can be eliminated by taking linear combinations of the form

$$|\phi_\rho; sM\rangle \equiv \sum_{K=-I}^{I} \hat{\Theta}_{MK}^s |F\rangle f_{K;\rho}. \tag{2.11}$$

In order to simplify the numerics, up to about two years ago a number of symmetry restrictions had been imposed on the general HFB transformation F: time-reversal and axial symmetry had been required, parity as well as proton–neutron mixing being neglected, and, last but not least, only real transformations F had been admitted.

According to Bloch and Messiah,[20] the HFB vacuum (2.5) then takes the canonical form

$$|F\rangle = \prod_{r=p,n} \left\{ \prod_{\pi=+,-} \left[\prod_{m=1/2}^{m_{\max}} \left(\prod_{\alpha}^{(\tau,\pi,m)} [u_\alpha + v_\alpha b_\alpha^\dagger b_\alpha^\dagger] \right) \right] \right\} |0\rangle, \tag{2.12}$$

where

$$b_\alpha^\dagger \equiv \hat{\tau} b_\alpha^\dagger \hat{\tau}^{-1}, \tag{2.13}$$

in which $\hat{\tau}$ is the time-reversal operator, and u_α and v_α are all real numbers with $u_\alpha \geqslant 0$ and $u_\alpha^2 + v_\alpha^2 = 1$ for all α.

The basic "building block" of the symmetry-restricted vacuum (2.12) can be represented as

$$b_\alpha^\dagger b_\alpha^\dagger = \sum_{i<k}^{(m_\alpha \tau_\alpha \pi_\alpha)} [1 + \delta(i,k)]^{-1} \sum_I (-)^{j_k + l_k - m_{\alpha_I}} \times (j_i j_k I | m_\alpha - m_\alpha 0) \{ D_{i\alpha} D_{k\alpha} [1 + (-)^I] \times [c_i^\dagger c_k^\dagger]_{12\tau_\alpha}^{I0} \}, \tag{2.14}$$

where D is the corresponding *real* first Bloch–Messiah transformation, which mixes in this case only states with the same m, τ, π quantum numbers, i denotes the triplet of quantum numbers n_i, l_i, j_i of the basis state, and the creators of the coupled two-nucleon states are given by

$$[c_i^\dagger c_k^\dagger]_{TT_z}^{IM} = \sum_{m_i m_k \tau_i \tau_k} (j_i j_k | m_i m_k M) (\tfrac{11}{22} T | \tau_i \tau_k T_z) c_i^\dagger c_k^\dagger. \tag{2.15}$$

Thus, the basic building block and hence the total vacuum, too, contains only "like"-nucleon pairs coupled to even angular momenta and positive parity. Therefore, using the above-mentioned symmetry restrictions, we can investigate only states with even angular momentum and positive parity in doubly even nuclei. However, we shall see in Secs. 3 and 4 that we can go rather far even with this symmetry-restricted *real* HFB transformation. Recently,[15,22,23] we succeeded in improving the approaches on the lines proposed in Ref. 21 by taking into account parity as well as proton–neutron mixing and admitting essentially *complex* mean fields. Only time-reversal invariance and axial symmetry are kept. Consequently, the now *complex* first Bloch–Messiah transformation D mixes all quantum numbers except m. It takes the form

$$b_\alpha^\dagger \equiv \sum_{i=1}^{M} \delta(m_i,m_\alpha)\, D_{i\alpha}^{*} c_i^\dagger; \quad m_\alpha > 0 \tag{2.16}$$

and

$$b_{\bar{\alpha}}^\dagger \equiv \sum_{i=1}^{M} \delta(m_i,m_\alpha)\, D_{i\alpha} c_i^\dagger; \quad m_\alpha > 0. \tag{2.17}$$

The corresponding "canonical" HFB vacuum takes the form

$$|F\rangle = \left\{ \prod_{m=1/2}^{m_{\max}} \left(\prod_{\alpha}^{(m)} [u_\alpha + v_\alpha b_\alpha^\dagger b_{\bar{\alpha}}^\dagger] \right) \right\} |0\rangle, \tag{2.18}$$

and its basic building block can be written as

$$\begin{aligned} b_\alpha^\dagger b_{\bar{\alpha}}^\dagger = & \sum_{\tau=p,n} \sum_{\mathrm{i}<\mathrm{k}}^{(m_\alpha \tau)} [1+\delta(\mathrm{i},\mathrm{k})]^{-1} \sum_I (-)^{j_k+l_k-m_\alpha} \\ & \times (j_i j_k I | m_\alpha - m_\alpha 0) \{ [\mathrm{Re}(D_{i_\tau \alpha}^{*} D_{k_\tau \alpha}) \\ & \times [1+(-)^{l_i+l_k+I}] + i\,\mathrm{Im}(D_{i_\tau \alpha}^{*} D_{k_\tau \alpha}) \\ & \times [1-(-)^{l_i+l_k+I}]] [c_i^\dagger c_k^\dagger]_{12\tau}^{I0} \} \\ & + \sum_{\mathrm{i}}^{(m_\alpha p)} \sum_{\mathrm{k}}^{(m_\alpha n)} \sum_{IT} (1/21/2T | -1/21/20) \\ & \times (-)^{j_k+l_k-m_\alpha} (j_i j_k I | m_\alpha - m_\alpha 0) \\ & \times \{ [\mathrm{Re}(D_{i_p \alpha}^{*} D_{k_n \alpha}) \times [1+(-)^{l_i+l_k+I}] \\ & + i\,\mathrm{Im}(D_{i_p \alpha}^{*} D_{k_n \alpha}) [1-(-)^{l_i+l_k+I}]] [c_i^\dagger c_k^\dagger]_{T0}^{I0} \}. \end{aligned} \tag{2.19}$$

It contains all possible two-nucleon couplings, including pairing correlations between like-nucleons as well as both the $T=0$ and the $T=1$ pairing correlations between protons and neutrons. Now states with arbitrary parity and angular momentum in both doubly even and doubly odd systems can be described.

With the basic ingredients of the theory being introduced, we shall now briefly review the variational procedures which have been used to investigate some even–even nuclei in the $A \sim 70$ mass region.

2.2. Variational procedures

Let us first assume that we are interested in the yrast state of a particular symmetry $s \equiv AT_z I^\pi$, e.g., the lowest $I^\pi = 8^+$ state in some even-mass nucleus. In this case one starts with a general HFB vacuum projected onto the desired symmetry quantum numbers as a trial wave function and extracts the underlying quasiparticle transformation via a variational calculation directly from the chosen effective many-body Hamiltonian. Minimizing the corresponding energy functional

$$E_1^s[F_1^s] = \frac{\langle \phi_1; sM | \hat{H} | \phi_1; sM \rangle}{\langle \phi_1; sM | \phi_1; sM \rangle} \tag{2.20}$$

with respect to arbitrary variations of the HFB transformation F_1^s, one obtains the optimal approximation to this state which can be reached by a single symmetry-projected HFB determinant. This is the VAMPIR[12] approach to this particular yrast state. Note that because of the symmetry projection before the variation the resulting transformation depends on the symmetry. Thus, already in this simplest approach, e.g., drastic changes of the structure with increasing spin can be described. The extension for the description of the excited states with the same symmetry is the EXCITED VAMPIR approach.[12–14] In this approximation excited states with the same symmetry, e.g., the first excited $I^\pi = 8^+$ state, are calculated in complete analogy, except that one has to ensure the orthogonality of the current trial wave function with respect to the VAMPIR solution. In other words, one eliminates the lowest solution for the considered symmetry from the variational space by Gram–Schmidt orthogonalization and then calculates the optimal approximation to the first excited state which can be reached again by a single symmetry-projected HFB determinant. If the first excited state is obtained, it is eliminated too, and then the second excited state is calculated, and so on, until m different symmetry-projected HFB determinants, optimal for the m lowest states of the considered symmetry, have been constructed.

Therefore we use as a trial wave function for the nth state ($n>0$) of a given symmetry the ansatz

$$|\varphi_n; sM\rangle \sim \sum_{i=1}^{n} |\phi_i; sM\rangle \beta_i^n = \sum_{i=1}^{n} \hat{\Theta}_{M0}^s |F_i^s\rangle \beta_i^n, \tag{2.21}$$

where the β_i^n are given by requiring normalization and orthogonality with respect to all the $(n-1)$ solutions already obtained and $|F_n^s\rangle$ is left free for the variation. Note that the variational calculation for each new determinant is completely independent of the one performed for any of the previous states with the same symmetry. Finally, the residual interaction in this basis of orthonormal A-nucleon configurations with the symmetry s is diagonalized and the final EXCITED VAMPIR wave functions are obtained:

$$|\Psi_\alpha^{(m)}; sM\rangle = \sum_{i=1}^{m} |\varphi_i; sM\rangle g_{i;\alpha}^{(m)s}. \tag{2.22}$$

However, using only one additional determinant for each new state to be considered, this approach is still a sort of mean-field approximation and may not always be sufficient, since the residual interaction between the m lowest configurations does not necessarily account for the dominant correlations on the top of each of the various EXCITED VAMPIR solutions. It may very well be that the dominant correlations to a main mean field for a given state are due to rather high-lying configurations, or due to configurations which have a completely different structure than those underlying the lowest m orthogonal A-nucleon solutions for a given symmetry.

An improved variational scheme incorporating such correlations in a systematic way, no matter where in energy they occur, the EXCITED FED VAMPIR approach[15,16,18] allows one to go beyond mean fields. The variational procedure performs as follows: for the yrast state of a given symmetry one starts again with the VAMPIR solution. Now one looks for a second symmetry-

projected determinant correlating this solution, but the main one is not taken out of the variational space. This is again obtained by a variational calculation, so that one always finds that configuration which yields the maximal additional energy for the considered yrast solution. After that a third determinant is constructed, etc., until a total of n_1 configurations have been obtained. The resulting correlated yrast state is then eliminated from the variational space, and the procedure is repeated for the first excited state with the same symmetry, and so on, until finally the m lowest states have been constructed. Thus, in this approximation the ith state of a given symmetry is represented as a linear combination of a few projected quasiparticle determinants constructed successively in a chain of variational calculations, the state being Schmidt-orthogonalized with respect to all the $i-1$ previously found solutions. In each step of the variational chain for the ith "correlated" wave function one varies only the last added mean field and the configuration mixing coefficients, which ensures the orthonormality of the resulting linearly independent solutions, asking for the maximum additional contribution to the energy of the previous approximation to that wave function. Such a properly normalized linear combination of n_i different HFB-type determinants $|F_k\rangle$ $(k=i,...,n_i)$ is created for the ith state of symmetry s:

$$|\Phi_i^{(n_i)};sM\rangle \equiv \hat{T}^{(i)}\hat{\Theta}^s_{M0}\sum_{\nu=1}^{n_i}|F_{q+\nu}\rangle f^{in_i}_{\nu,1} \equiv \hat{\Theta}^s_{M0}\sum_{j=1}^{\omega(i)}|F_j\rangle\eta^i_{j,1}, \tag{2.23}$$

where $\hat{T}^{(i)}$ eliminates the first $i-1$ solutions from the model space, q indicates the total number of building determinants, $q\equiv\Sigma_{j=1}^{i-1}n_j$, and $\omega(i)\equiv\Sigma_{i=1}^{i}n_i$. Finally, as already in the EXCITED VAMPIR approximation, the residual interaction between the m energetically lowest linear combinations is diagonalized, and the lowest m physical states of symmetry s,

$$|\Psi_\alpha^{(m)};sM\rangle = \sum_{i=1}^{m}|\Phi_i^{(n_i)};sM\rangle g^{(m)}_{i\alpha}, \quad \alpha=1,...,m, \tag{2.24}$$

and the corresponding energies $E_\alpha^{(m)}$ $(\alpha=1,...,m)$ are obtained:

$$(H-E^{(m)}\mathbf{1})g^{(m)}=0, \quad g^{(m)\dagger}g^{(m)}=\mathbf{1}_m. \tag{2.25}$$

The EXCITED FED VAMPIR variational procedure, going beyond the symmetry-projected quasiparticle mean-field approximations, automatically selects the relevant degrees of freedom for the main mean field underlying the structure of a particular state, and also accounts for the most important additional correlations with respect to the approximation already obtained. In this way arbitrary drastic changes of the structure with increasing excitation energy or spin are accessible, and, furthermore, various types of shape coexistence could be distinguished. These particular features of this model are essential for an adequate description of the structure of nuclei displaying a dynamical shape coexistence. The improvement with respect to the EXCITED VAMPIR approximation comes from the fact that the dominant correlations on top of the optimal projected mean-field solutions are incorporated for each state separately. In this way each of the still neglected configurations could bring to the energy for the already obtained states only gains comparable with that from the last correlating configuration included for any of them. Also, the residual interaction will be at most at this level, and of course much smaller, and thus the confidence level of the resulting wave functions is improved.

Of course, the complex versions of the VAMPIR, EXCITED VAMPIR, FED VAMPIR and EXCITED FED VAMPIR approaches (later referred to as CV, CEV, CFV, and CEFV, respectively) represent a remarkable improvement with respect to their *real* restricted partners (RV, REV, RFV, and REFV). This will be exemplified below by recently obtained results concerning new aspects of the shape coexistence at low excitation energies in an even–even $N=Z$ system.

2.3. The model space and the effective interaction

Calculations in the $A\sim70$ region within the *real* versions of the EXCITED VAMPIR and EXCITED FED VAMPIR approximations have been performed using a rather large model space: the full $N=3$ and $N=4$ shells for both protons and neutrons, and, for the latter, in addition the $0h_{11/2}$ orbital. As an effective two-body interaction a Brueckner nuclear-matter G matrix derived from the Bonn OBEP (Ref. 24) was taken, which was renormalized by adding two short-range (0.7 fm) Gaussians with strengths of -50 MeV and -40 MeV to the $T=1$ proton–proton and neutron–neutron relative matrix elements, respectively, introduced to enhance the pairing components. An isospin-independent spin–orbit Gaussian was added, and, finally, the onset of deformation was influenced by a monopole shift in all the diagonal $T=0$ matrix elements of the form $\langle 0g_{9/2}0f;IT=0|\hat{G}|0g_{9/2}0f;IT=0\rangle$, where $0f$ denotes either the $0f_{5/2}$ or the $0f_{7/2}$ orbit. The single-particle energies were adjusted in MONSTER (HFB) calculations[12] for "well deformed" odd-mass nuclei in the $A\sim50$ and $A\sim80$ mass regions. The Hamiltonian defined in this way was then kept fixed and used for EXCITED VAMPIR and EXCITED FED VAMPIR calculations in several doubly even Ge, Se, and Kr isotopes.

For the corresponding *complex* calculations 72 single-particle states above the ^{40}Ca core (the same core as for the *real* calculations) were available for the (about 30) valence nucleons. Here the $1p_{1/2}$, $1p_{3/2}$, $0f_{5/2}$, $0f_{7/2}$, $1d_{5/2}$, and $0g_{9/2}$ oscillator orbits for both protons and neutrons were taken as a model space. Consequently, a slightly modified monopole shift for the above-mentioned $T=0$ matrix elements was used in the normalization of the G matrix.[23]

3. SHAPE COEXISTENCE IN THE $A\sim70$ REGION WITHIN THE *REAL* EXCITED VAMPIR APPROACH

The basic idea of the EXCITED VAMPIR approach is to obtain optimized mean fields for each state of a given symmetry separately. In a chain of variational calculations for projected determinants, starting from the lowest state for a given angular momentum and parity I^π, and then

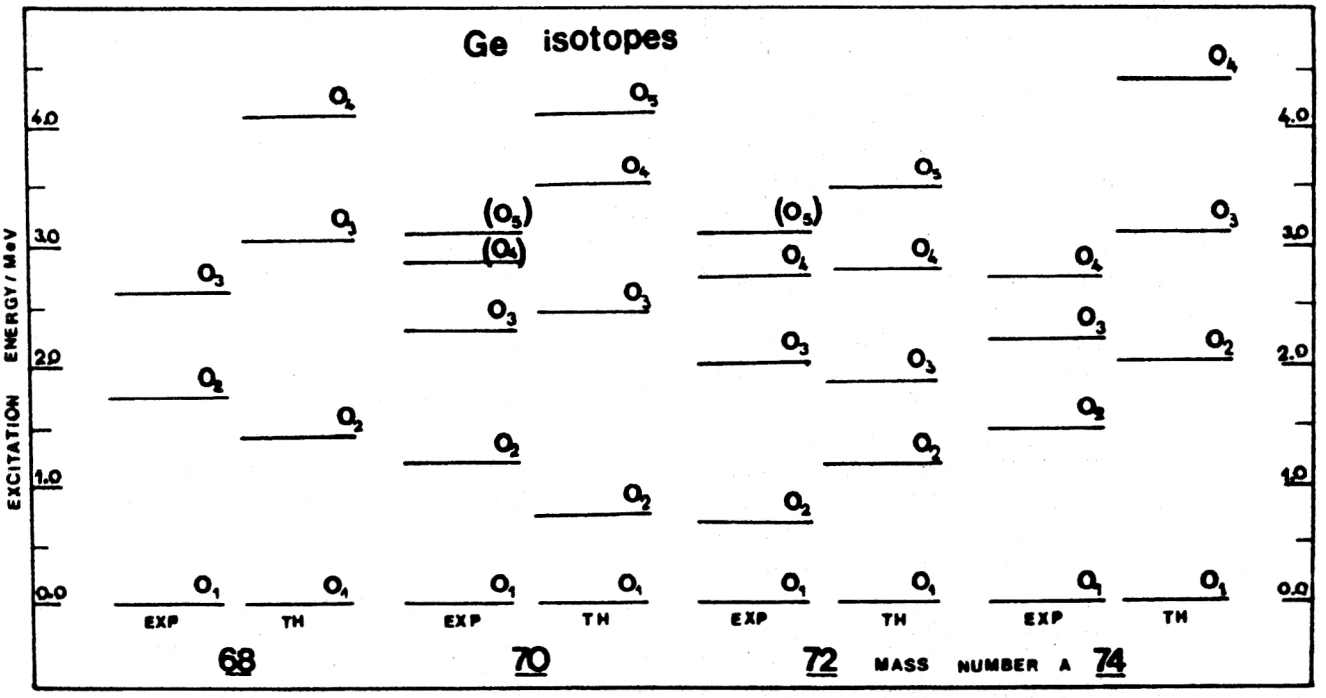

FIG. 1. Comparison of theoretical and experimental energy trends for the 0^+ states in the investigated Ge isotopes.

stepping up from one state to the next lowest one for the same I^π, with the current trial wave function always constrained to be orthogonal to all the solutions already obtained, one can describe states of very different structure. Therefore this approach should also allow one to describe the shape coexistence which is suggested by the data in the Ge and Se nuclei. One could even say that the complex situation encountered in the $A\sim70$ region is a challenging testing ground for this theoretical model.

3.1. Low-spin states in even–even Ge and Se isotopes

The first insights into the complex structures of the nuclei in the $A\sim70$ mass region came from the investigation of the low-spin states in some chains of even Ge and Se nuclei in the framework of the *real* EXCITED VAMPIR model.[13] This approach indeed always yields, in all the considered doubly even Ge and Se isotopes, some low-lying 0^+ and 2^+ states in the first few MeV of excitation energy, as observed experimentally. In Fig. 1 we show the energies of all the calculated and experimentally known 0^+ states in the ^{68,70,72,74}Ge isotopes. The maximum number of A-nucleon REV configurations for one angular momentum built by the EXCITED VAMPIR variational procedure was five. One obtains VAMPIR wave functions, which are orthogonalized to each other, in various local minima. The $A\sim70$ region is a good example to illustrate the power of this EXCITED VAMPIR method, since one expects, owing to the various gaps in the Nilsson spectrum, minima at rather different deformations. As a first state in a successively created optimal basis of A-nucleon configurations, the most bound from the projected determinants so produced is taken. For the next states of the form (2.21) the variational principle guides us to choose the nth projected determinant. Diagonalizing the residual interaction within the lowest m variational states, one obtains the best possible description of the m lowest states of the considered spin value, which can be achieved by m projected HFB-type quasiparticle determinants. Of course, increasing the number of successive solutions m, we improve the structure of any wave function of the type (2.22), since the diagonalization of the residual interaction between more orthogonal states introduces more correlations in the final REV wave functions.

To get an idea about the structure of the *real* EXCITED VAMPIR wave functions for low-spin states in the investigated Ge and Se isotopes, we display in Figs. 2 and 3 some typical information. In these figures we show for all REV 0^+, 2^+, and 4^+ states in ^{70,72}Ge nuclei the intrinsic quadrupole moments for both neutrons (circles) and protons (squares) for the ith projected determinant $|\phi_i^s\rangle$, and for the 2^+ and 4^+ states the corresponding values calculated from the spectroscopic quadrupole moments of the physical states. Owing to the strong mixing of prolate and oblate projected determinants in the final wave functions, the intrinsic quadrupole moments are often drastically reduced with respect to those of the projected nonorthogonal determinants. Moreover, even the sign of the intrinsic quadrupole moment for a state may appear changed with respect to that for the corresponding dominant determinant of the ith variational solution, as is the case for the second, third, and fourth 2^+ states in ^{70}Ge and the second 2^+ state in ^{72}Ge. The nature of each projected determinant included in the calculations for a given symmetry s is pictured in Figs. 2 and 3 by the intrinsic quadrupole and

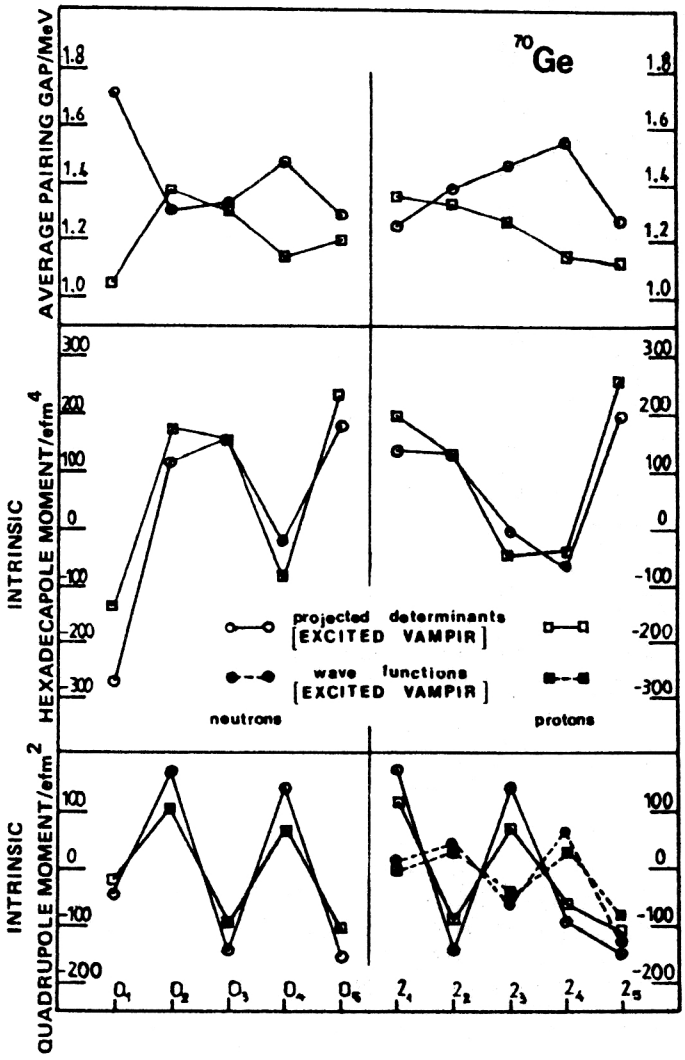

FIG. 2. The intrinsic neutron and proton quadrupole and hexadecapole moments of the lowest five projected quasiparticle determinants obtained by the REV procedure for the 0^+ and 2^+ states in ^{70}Ge, and the intrinsic quadrupole moments obtained from the corresponding spectroscopic value for the final REV wave functions [Eq. (2.22)] (full symbols are used). No effective charge has been used. The average neutron and proton pairing gap is given also for the above specified determinants. Squares refer to the proton, circles to the neutron, and open symbols are for projected determinants.

hexadecapole moments and the average pairing gaps. The above-mentioned quantities are given for both neutrons and protons. The average pairing gaps are defined here in the usual way[25] as mean eigenvalues of the corresponding HFB pairing matrices $\Delta(\tau)$:

$$\Delta^{\tau}_{\text{aver}} \sim (1/M_{\tau})\text{tr}\Delta(\tau), \tag{3.1}$$

where

$$[\Delta(\tau)]_{ik} \sim \frac{1}{2} \sum_{r,s}^{(\tau)} v(ikrs)(B^{*}A^{T})_{rs} \tag{3.2}$$

is the (M_{τ} by M_{τ}) pairing matrix; A and B are the HFB transformation matrices of Eqs. (2.2) and (2.3).

The shape coexistence in the Ge isotopes is corroborated by our results. A tendency from an almost pure oblate slightly deformed 0^+ ground state in ^{68}Ge to a strongly mixed prolate–oblate one in ^{72,74}Ge is predicted. For the ground states of the studied Se nuclei a tendency to an increasing prolate mixing going from 72 to 74 isotopes can be observed. For the excited 0^+ states both Ge and Se isotopes reveal a strong prolate–oblate mixing.

More information about the structure of the ground and the first two excited 0^+ states can be obtained from the spherical occupations of both neutron and proton orbitals illustrated in Figs. 4 and 5. From the trend of the proton and neutron spherical occupation number we can learn more about the similarities and the differences concerning the structure of a particular state in a chain of isotopes, and we can also easily compare these properties for a given symmetry s in a chain of isotopes. The theoretical results for the proton-number occupations for the ground state in the considered Ge and Se isotopes are in good agreement with the experimental results obtained from (d, ^{3}He) transfer reactions on Ge and Se targets[26,27] and also from (p,t) reactions.[28–30]

Besides the energies of the low excited low-spin states, and the neutron and proton spherical occupations for 0^+ states, in these calculations the dependence of the deformation on the mass number as manifested in the spectroscopic quadrupole moments of the 2^+ yrast states and the $E0$ transition probabilities between the first excited 0^+ states and the ground states could also be accurately taken into account. The general trends in the quadrupole moments and $E0$ transition probabilities are in fair agreement with the available experimental data,[31–33] as can be seen from Figs. 6 and 7.

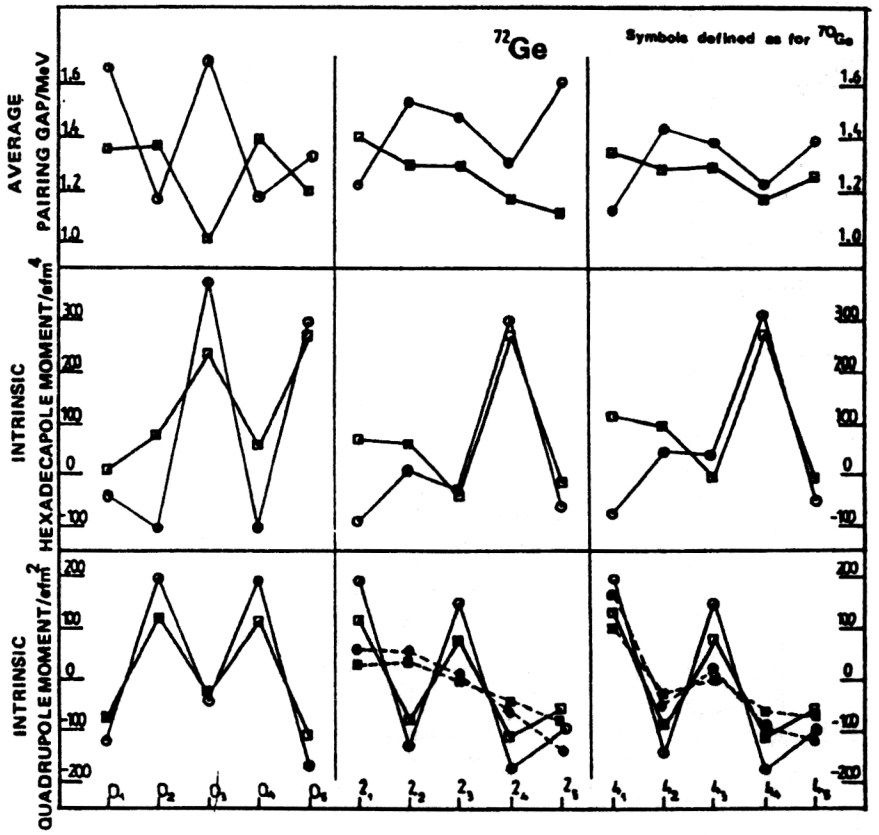

FIG. 3. The same as in Fig. 2, but for the calculated 0^+, 2^+, and 4^+ states in ^{72}Ge.

Indeed, the EXCITED VAMPIR approach is able to describe the shape-coexistence phenomena very nicely. The results indicate that for low angular momenta configurations with different deformations not only "coexist" but mix strongly with each other. The REV wave functions for the low-spin states in this mass region are in general complicated mixtures of several configurations corresponding to rather different deformations, with a special interplay of

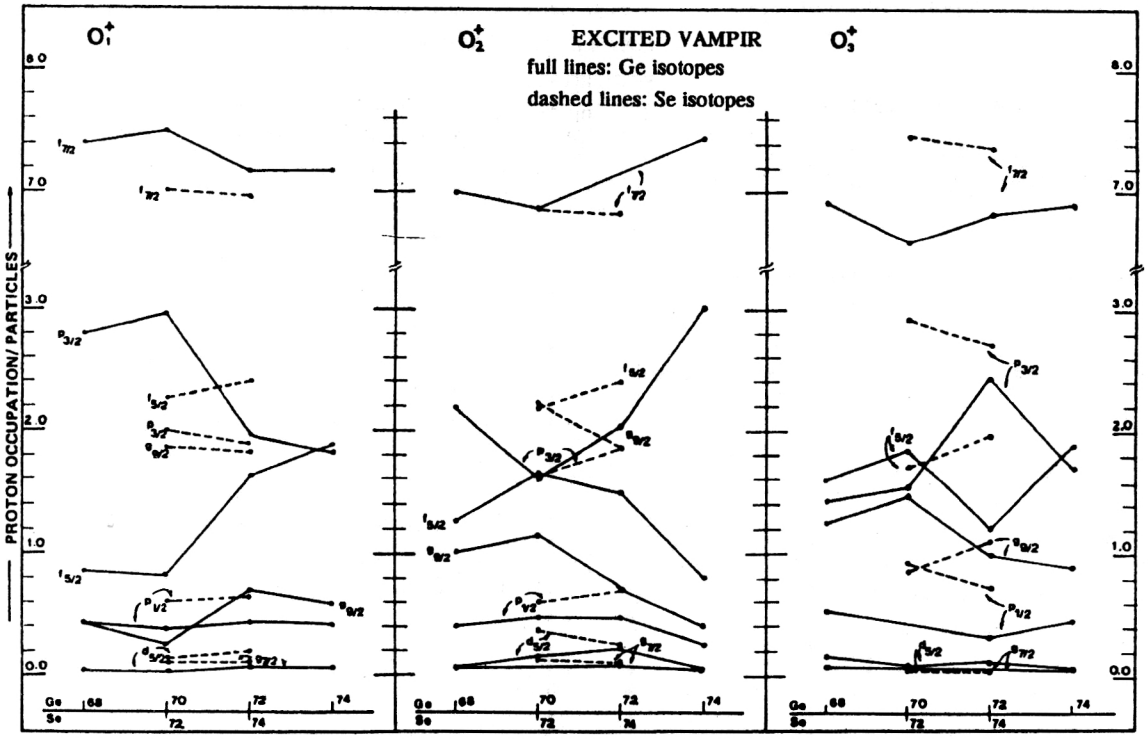

FIG. 4. Significant proton occupation numbers of the spherical-basis orbitals for the lowest three 0^+ states in the investigated Ge and Se isotopes. Full lines are for Ge nuclei; dashed lines, for Se nuclei.

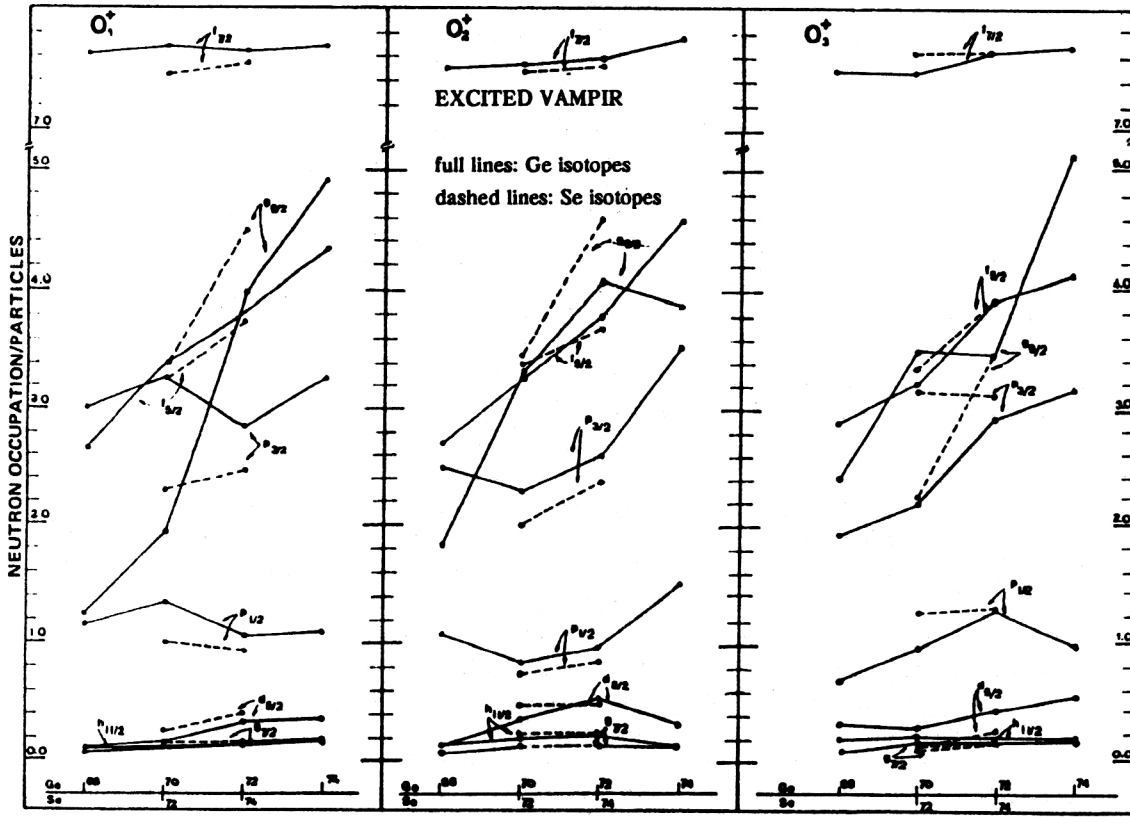

FIG. 5. The same as in Fig. 4, but for the neutron occupations.

the prolate and oblate deformed mean fields and dynamical changes of the hexadecapole deformations. This holds especially for the 0^+ states; however, though with decreasing importance, considerable mixing is obtained also in the 2^+ and 4^+ states.

3.2. High spins in ^{68}Ge, ^{70}Se, and ^{72}Se nuclei

These encouraging results and the experimental evidence concerning the triple forking at 8^+ into three bands with no crossing transitions observed earlier[34] gave us motivation to extend our studies to states with higher angular momenta to investigate whether the shape coexistence does persist also at high spins. In the framework of the *real* EXCITED VAMPIR approximation we extended our investigations to spins up to 18^+ in ^{68}Ge and ^{70}Se, and up to 22^+ in ^{72}Se. Note that these calculations have been made using the same model space and effective Hamiltonian as for the low-spin states.

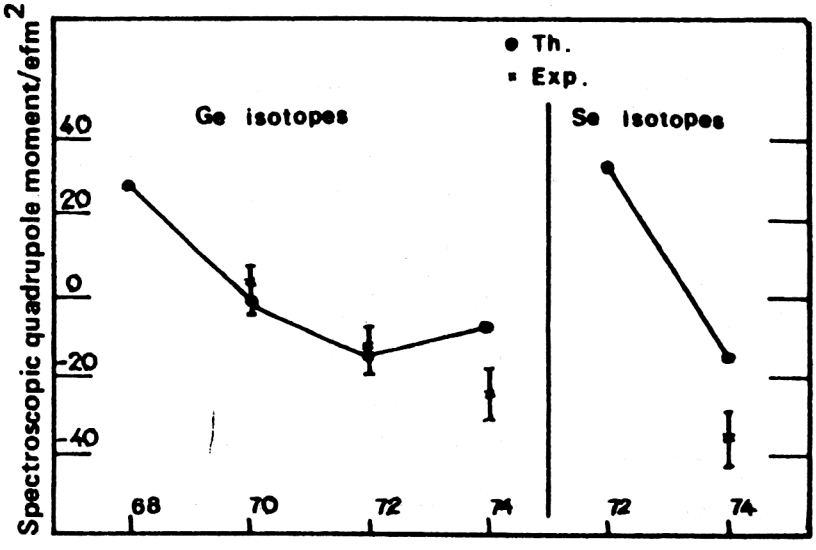

FIG. 6. Comparison of the theoretical spectroscopic quadrupole moments for the first 2^+ states in the investigated Ge and Se nuclei and the corresponding available data. The effective charge is $e_n=0.25$ and $e_p=1.25$.

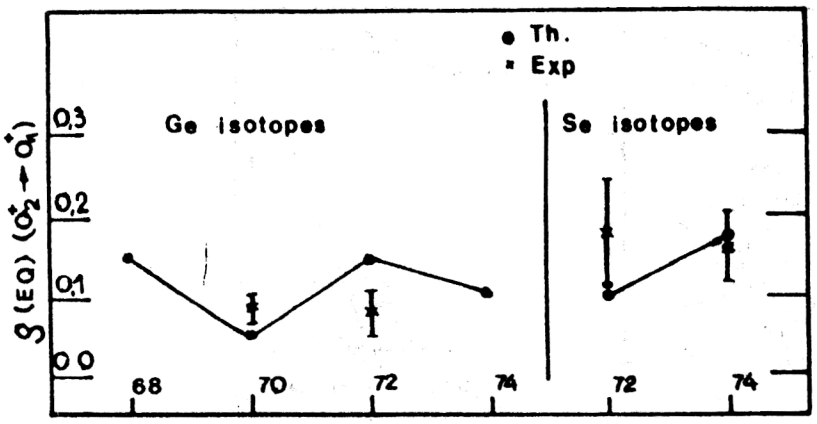

FIG. 7. Comparison of the theoretical $E0$ transitions $\rho(E0;0_2^+ \to 0_1^+)$ in the investigated Ge and Se nuclei with the corresponding available data. Effective charges $e_n=0.25$ and $e_p=1.25$ have been used.

For the description of the structure of the high-spin states up to $m=8$, A-nucleon EXCITED VAMPIR configurations of the type (2.21) for each considered angular momentum were taken into account. It turned out that the *shape coexistence*, i.e., the occurrence of various states with the same spin based on configurations with different deformations within a small interval of excitation energy, indeed persists even at rather high spin values.

As expected from the different gaps characterizing the Nilsson scheme for the nuclei in the $A\sim 70$ mass region, we obtained for each considered spin many different HFB-type projected determinants corresponding to very close-lying local minima. These determinants can differ, e.g., in the sign and/or magnitude of the intrinsic quadrupole moments, or, in some cases, e.g., only in the sign and/or magnitude of the intrinsic hexadecapole moments, which play a very special role in all three nuclei ^{68}Ge, ^{70}Se, and ^{72}Se, favoring in some cases the alignment of the neutrons occupying the spherical $g_{9/2}$ state.

The orthogonal variational states (2.21) produced by the REV procedure and finally the physical states (2.22) obtained by the diagonalization of the residual interaction are still very close in energy. In all three nuclei we have obtained 4–5 states of a given spin (8^+, 10^+, 12^+, 14^+), bunched within only 1.5 MeV. The theoretical results presented in Fig. 8 for ^{68}Ge and in Figs. 9 and 10 for ^{70}Se and ^{72}Se, respectively, reveal a special feature: most of the high-spin states decay in many different ways. Note that the experimental spectrum given in Fig. 8 for ^{68}Ge was the only one available at the time when we accomplished our

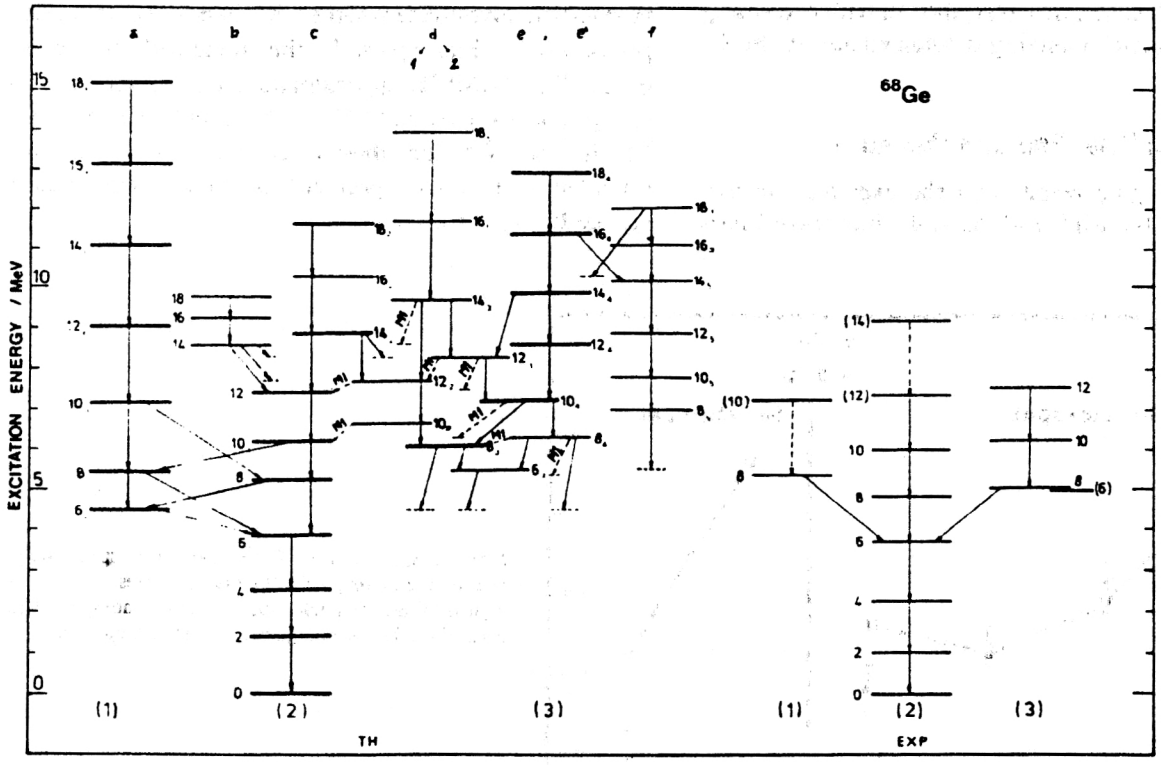

FIG. 8. The theoretical spectrum of the nucleus ^{68}Ge obtained here in the real EXCITED VAMPIR approximation, compared with the experimental data of de Lima *et al.*[34]

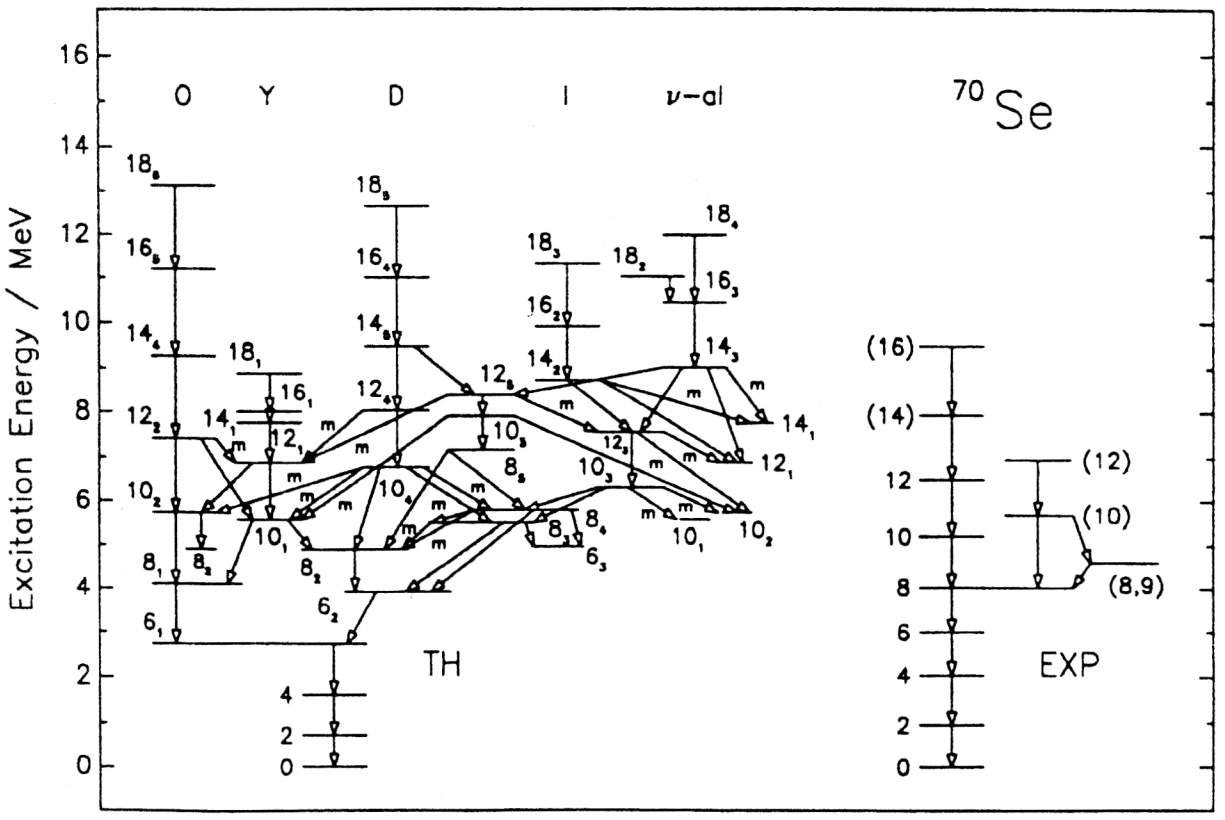

FIG. 9. The theoretical spectrum for ^{70}Se obtained within the *real* EXCITED VAMPIR approach, compared with the available experimental data.[35,36] The labels indicating the classification of the various theoretical bands are explained in the text, and the symbol *m* at some of the decay links refer to strong $\Delta I=0$ $M1$ transitions.

REV calculations. Recent experimental data[17] support our predictions. These will be presented later and compared with the results of more sophisticated investigations using the *real* EXCITED FED VAMPIR approach.

We analyzed all the possible decay paths starting from the states with the highest calculated spin in each nucleus. Since we have so many states for each spin bunched so much in energy, decaying by many branches, and since the measured $B(E2)$ values reported by different experimental groups have a large spread and involve large error bars which arise from the uncertainties associated with the feeding times, we can always suggest a few "most probable" paths of the cascades leading to the yrast 6^+ state which are compatible with the presently available experimental data. The situation becomes even more complicated, since we found strong $M1$, $\Delta I=0$ transitions which in some cases are much faster than the intraband $E2$ transitions. We classified the calculated levels into different collective bands solely on the basis of the $B(E2)$ values among them. Then for all three nuclei we tried to find the fastest ways to enter the yrast line and so to identify the most probable candidates for the experimental linkages of the measured gamma rays in bands.

In all three nuclei an oblate band (always the one at the extreme left spectrum) coexists with many other prolate bands. For the higher spins the oblate bands consist of the highest calculated states of a given angular momentum. In the theoretical spectra the label for each spin corresponds to the energy order in the calculated set of states for a given angular momentum.

In ^{68}Ge the yrast band is mainly oblate up to spin 6^+. The strongest oblate–prolate coexistence is obtained for the first two 8^+ states. Starting with spin 10^+ a pure oblate band emerges, coexisting with all the other prolate bands. No feeding from this oblate band to the prolate bands exists above spin 10^+. With respect to the other calculated bands, however, these oblate states are at rather high excitation energy and are therefore probably only weakly populated. Concerning the other bands presented in Fig. 8, these are pure prolate bands for spins $I\geqslant 10$. The structure of the wave functions for the $I^\pi=10^+$, 12^+, 14^+ states shows a rather strong mixing of various mean fields differing by the neutron and proton intrinsic quadrupole and hexadecapole deformations. This shape coexistence explains the appearance of two or three comparable fast transitions for the decay of a given state, as can be seen in Fig. 8, which was later confirmed by experiment (Fig. 23). The various mean fields dominating the structure of the wave functions for the other spins also have different neutron and proton intrinsic quadrupole and hexadecapole moments. Protons and neutrons contribute equally to the special structure of the high-spin bands. In Fig. 11 we display the proton and neutron intrinsic quadrupole moments for the three fastest decaying prolate bands and for the oblate

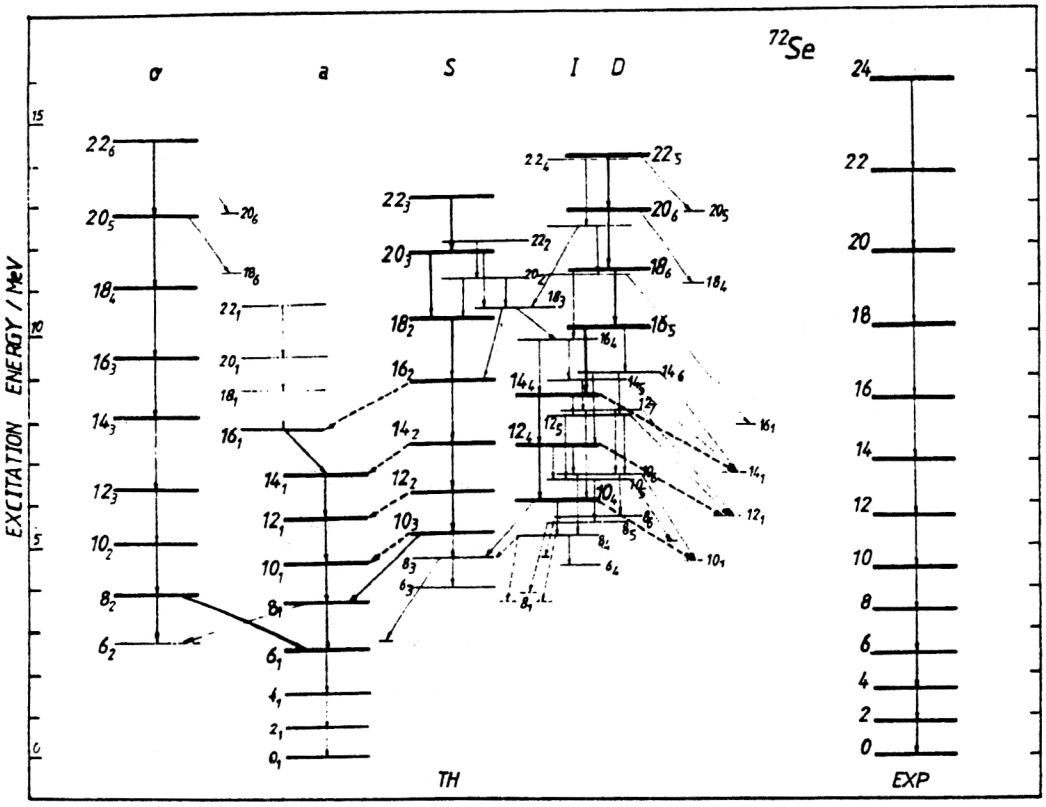

FIG. 10. The theoretical spectrum for ^{72}Se obtained in the *real* EXCITED VAMPIR approximation, compared with the experimental data.[17,36] The labels of the theoretical bands are explained in the text, and the dashed lines indicate strong $M1$ $\Delta I=0$ transitions.

band. The labels of the bands are the same as in Fig. 8.

A measure of the deformation characterizing the different bands is offered by the theoretical and experimental evaluated $B(E2,\Delta I=2)$ values[34,37–39] given in Table I. The agreement of the theoretical $B(E2)$ values with the experimental data is rather poor, even if one takes into account the large error bars and the large spread in these data obtained by different groups. As the side feeding in this mass region is still an open problem,[4] we did not intend to fit these data. Therefore for all the investigated nuclei the same values of the effective changes and the same renormalization of the effective Hamiltonian were used.

In Fig. 12 we give the neutron and proton intrinsic hexadecapole moments of the bands calculated in ^{68}Ge in the REV approximation. A special trend is displayed by the d_1 band, which is in fact a neutron-aligned band: for the 8_3^+ state the hexadecapole moments are much smaller than for the 8_1^+ and 8_2^+ states, and the neutron Q_4 moment is negative. Except for the 12_2^+ state, which still has the smallest hexadecapole moments of all displayed 12^+ states, the neutron and proton Q_4 moments are negative for all the higher spin states of the d_1 band. A qualitative understanding of the effect of hexadecapole deformation on the orbitals lying around the Fermi level can be obtained in the framework of a simple perturbation treatment applied on a Nilsson-type axially deformed potential including a Y_{40} deformation.[41] The wave functions for the 10^+, 14^+, 16^+, and 18^+ spin states belonging to the d_1 band are based essentially on a single VAMPIR determinant, prolate deformed, with the smallest observed quadrupole deformation for both neutrons and protons, slowly decreasing with increasing spin. The 8_3^+ and 12_2^+ states of the d_1 band are mixed states based on coexisting mean fields with positive and negative hexadecapole moments. The contribution of the $g_{9/2}$ neutrons to the intrinsic hexadecapole moment is very small in the d_1 band and even becomes negative for some spins. For the case of a negative hexadecapole moment the simple perturbation treatment predicts that the $m=1/2$ $g_{9/2}$ orbital moves to the Fermi level favoring the alignment of the two neutrons occupying the spherical $g_{9/2}$ state. This effect can also be seen in our wave functions. The proton occupation of the $g_{9/2}$ orbital slowly goes down to zero with increasing spin for d_1 band states, and consequently a sharp alignment of the neutrons is very much favored. This strong neutron alignment is reflected in the small g factors of the states belonging to the d_1 band, which even become negative for the spin 8^+ and 10^+ states. Therefore, it is rather likely that the 8_3^+ state corresponds to the experimental 8_2^+ state, for which a g factor of -0.28 ± 0.14 has been measured.[42]

A picture revealing a possible sharp alignment of the angular momenta of the particles occupying the high-j spherical orbital ($g_{9/2}$ for the $A\sim 70$ region) with respect to the total angular momentum is given in Fig. 13. The normalized angular-momentum contribution of the $g_{9/2}$ neutrons and protons in the direction of the total angular momentum **I** is given by

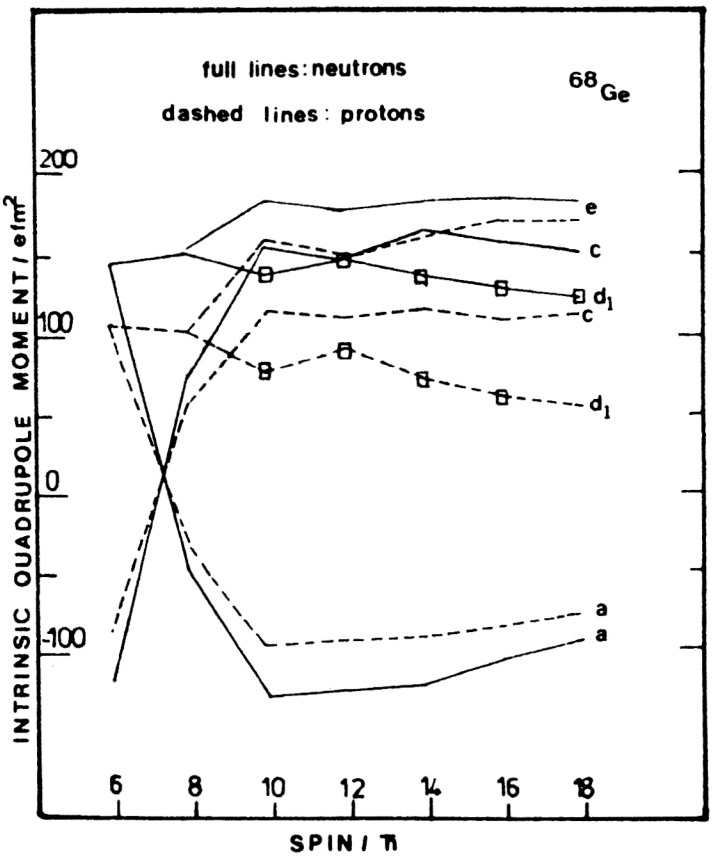

FIG. 11. The intrinsic neutron and proton quadrupole moments obtained from the corresponding spectroscopic values for the states belonging to the specified (a,c,d_1,e) bands in ^{68}Ge in the REV approximation. No effective charge has been used. Full lines are for neutrons; dashed lines, for protons.

$$J(\tau nlj)=\frac{\langle\Psi;sM|\hat{\mathbf{J}}(\tau nlj)\cdot\hat{\mathbf{I}}|\Psi;sM\rangle}{\sqrt{I(I+1)}}. \qquad (3.3)$$

In Fig. 13 we present the resulting alignment plots (bottom part) and the occupation numbers (upper part) for the neutrons (left) and protons (right) filling the $g_{9/2}$ spherical single-particle state. A sharp alignment of the neutrons is evident in going from the 6_2^+ to the 8_3^+ state. This strong alignment dominates the d_1 band. Except for the 12^+ state the neutron occupation number is very close to two particles for all the states belonging to this band. At the same time the protons from the $g_{9/2}$ orbital almost do not contribute to the total angular momentum of the states. This can be understood from the continuous depletion of this orbital with increasing spin. This is a normal trend created by the gradual decrease of the intrinsic quadrupole moment, well distinguished in Fig. 11. A sharp proton alignment characterizes the yrast band (c) going from spin 6 to 10. For higher spins in this band, protons and neutrons make a comparable moderate contribution to the total angular momentum. The alignment of the particles in the $g_{9/2}$ orbital is reflected by the g factors plotted in Fig. 14.

Our calculations revealed some strong $B(M1,\Delta I=0)$ transitions for ^{68}Ge, indicated in Fig. 8 by dashed lines. Predicted by Frauendorf in the framework of the cranked shell model[43] and measured by Funke *et al.*[44] in even and

TABLE I. Some calculated (REV) and experimental[34,37–39] $B(E2,I_i\to I_f)$ (e^2fm^4) values for the nucleus ^{68}Ge. The effective charges were $e_n=0.25$ and $e_p=1.25$.

I_i	I_f	Theory	Experiment		
			a)	b)	c)
2	0	181	251^{+126}_{-63}	150^{+100}_{-56}	129±30
4	2	633	177^{+64}_{-37}	221^{+70}_{-60}	204±110
6	4	834	197^{+78}_{-44}	196±50	>137
8_y	6_y	503	281^{+70}_{-47}	600^{+100}_{-130}	220±60
8_r	6_y	3	260±100		
8_l	6_y	395	50±20	79±30	
10_y	8_y	811	410±110	457^{+114}_{-130}	760^{+380}_{-300}

y — yrast, l — left and r — right bands in Fig.8.
a) ref. [34,37], b) ref. [38], c) ref. [39].

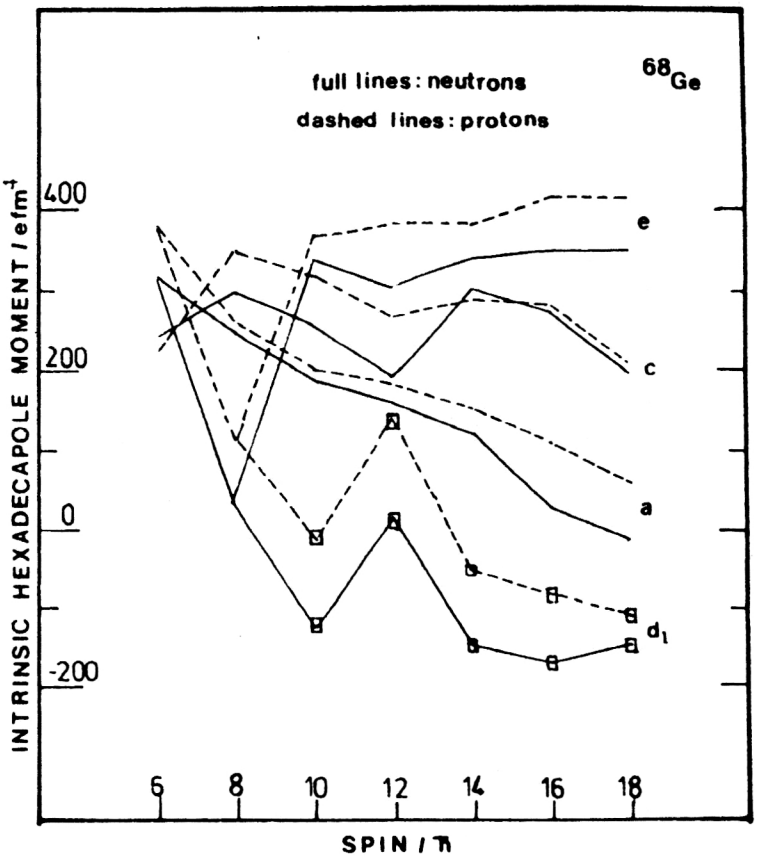

FIG. 12. The intrinsic neutron and proton hexadecapole moments obtained from the corresponding calculated values in the laboratory system for the states belonging to the specified (a,c,d_1,e) bands in ^{68}Ge in the REV approximation. No effective charge has been used. Full lines are for neutrons; dashed lines, for protons.

odd Kr isotopes, such strong $\Delta I=0$, $M1$ transitions between states of crossing bands should be expected. All these strong $M1$ transitions are dominated by $g_{9/2}$–$g_{9/2}$ recoupling terms, i.e., they result mainly from a reordering of the particles in this orbit in the final state with respect to the initial state. Spin and orbital contributions to the transition amplitudes are of about the same size with, in general, a slight dominance of the latter. Thus, e.g., in the largest $M1$ transition $[B(M1)=2.56\mu_N^2]$, connecting two 8^+ states, the total transition amplitude is $-6.60\mu_N$. From this value we have $-2.23\mu_N$ from the neutron-spin and $-0.84\mu_N$ from the proton-spin parts. The proton orbital

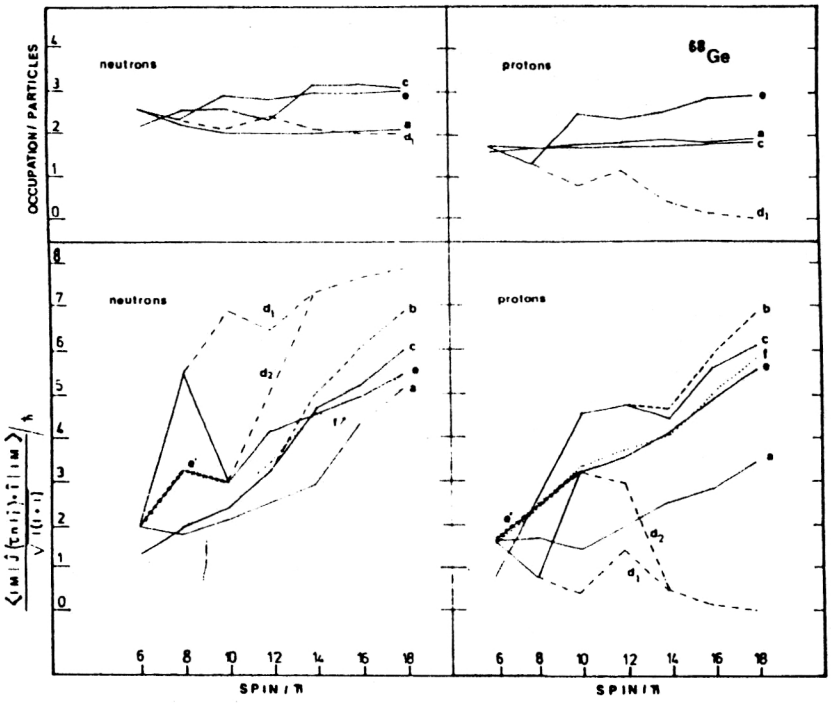

FIG. 13. The alignment plot (bottom part) representing the normalized angular-momentum contribution of the neutrons (left) and protons (right) filling the $g_{9/2}$ spherical basis state in the direction of the total angular momentum **1** for the positive-parity states of the REV bands calculated in ^{68}Ge. In the upper part of the figure the neutron (left) and the proton (right) occupation numbers of the spherical $g_{9/2}$ for some of the theoretically obtained bands in ^{68}Ge are given.

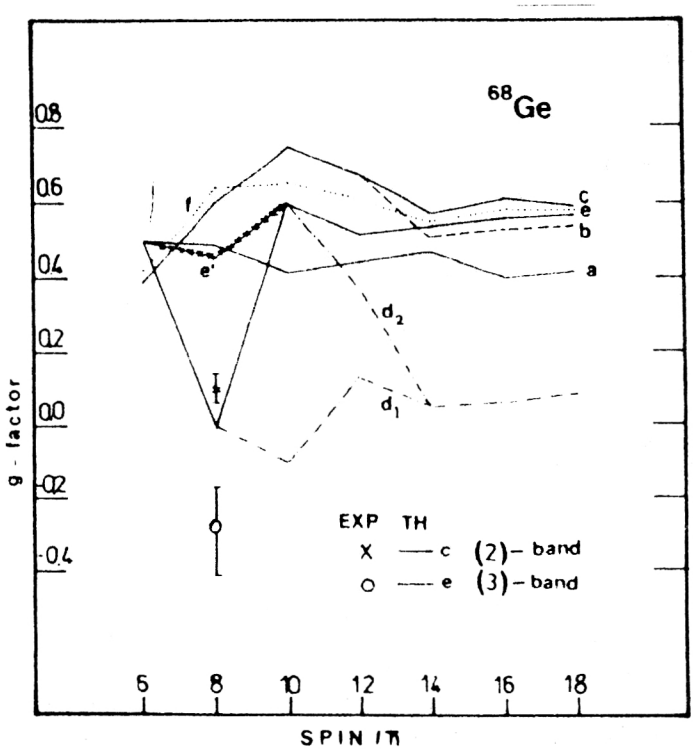

FIG. 14. The g factors of the REV bands in ^{68}Ge and the available data for some 8^+ states. The calculated bands labeled c and e are associated with the experimental bands classified as (2) and (3), respectively. Free values for the neutron and proton g factors have been used in the calculations.

contribution, on the other hand, is $-3.63\mu_N$. The latter value can be decomposed into $-2.04\mu_N$ from the diagonal $g_{9/2}$, $-0.82\mu_N$ from the diagonal $f_{7/2}$, and $-0.52\mu_N$ from the diagonal $f_{5/2}$ single-particle transition matrix elements (the rest is distributed over many different spectroscopic amplitudes). These strong $M1$ transitions are an interesting result of the calculations. These predictions concerning the fast $M1$ transitions complete the picture of the most probable paths of feeding the investigated states.

We shall now consider the nucleus ^{70}Se, which has two more protons than the nucleus ^{68}Ge. The investigations of the features of ^{70}Se have been performed in the framework of the *real* EXCITED VAMPIR approximation, using the same model space and effective Hamiltonian as above. Here we have calculated the lowest six 0^+, 2^+, 8^+, 10^+, 12^+, 14^+, 16^+, and 18^+ as well as the lowest five 4^+ and 6^+ states, and after the diagonalization of the residual interaction the solutions have been grouped again into various bands entirely on the basis of the $B(E2)$ values. A rather complicated decay pattern with a high level density in a certain spin region can be seen in the spectrum given in Fig. 9. The structure of the various bands can be summarized as follows:

Up to angular momentum 8^+ the yrast states are almost pure oblate configurations. This oblate band O then continues with the second 10^+ state, which, however, has a strongly mixed wave function with a large prolate component. Above the second 12^+ state, which still displays some oblate–prolate mixing, the band then continues with the fourth 14^+, the sixth 16^+, and again the sixth 18^+ solutions, which again have rather pure oblate deformed configurations. As in ^{68}Ge, the protons and neutrons in the $0g_{9/2}$ shell-model orbit both contribute little to the total angular momentum of this oblate band, as can be seen from Fig. 15, where the corresponding alignments are plotted.

The other four bands displayed in Fig. 9 are again all prolate-deformed, as can be seen from the spectroscopic quadrupole moments in Table II. Most of them also have a structure similar to the bands of ^{68}Ge discussed above. The band labeled D is strongly deformed (the dominant determinant in the 14_5^+ state having a quadrupole deformation $\beta_2 \sim 0.32$). The neutron-aligned band ν–al is a moderately deformed band, and the $0g_{9/2}$ neutrons are responsible for a considerable portion of the total angular momentum. As a consequence, the g factors in this band are distinctly smaller than in all the other bands being presented. As compared with the case of ^{68}Ge, however, the neutron alignment in the ^{70}Se band is less pronounced. This is due to the fact that in the ^{68}Ge band there are just two $0g_{9/2}$ neutrons, while the proton $0g_{9/2}$ orbit is almost empty. Thus, the neutron alignment is very much favored. In ^{70}Se, however, we have two additional protons which partly occupy the $0g_{9/2}$ orbit and also lead to a somewhat larger neutron occupation of this level. Thus, here the alignment does not happen as rapidly as in the former case. Adding two more neutrons, the occupation of the $0g_{9/2}$ orbit is increased even more, the alignment is severely hindered, and this is the reason why no equivalent band was found in the case of ^{72}Se, which will be discussed below. As a consequence of the less pronounced alignment, the neutron-aligned band in ^{70}Se starts with a g factor of still 0.24 for the 10_3^+ solution, while in ^{68}Ge the g factor of the 8_3^+ band head was even reduced to -0.03. Parallel to the neutron-aligned band, another moderately deformed prolate band labeled I in Figs. 9 and 15 and in Table II is obtained. Below angular momentum 14 these two bands, having rather similar spectroscopic quadrupole moments and

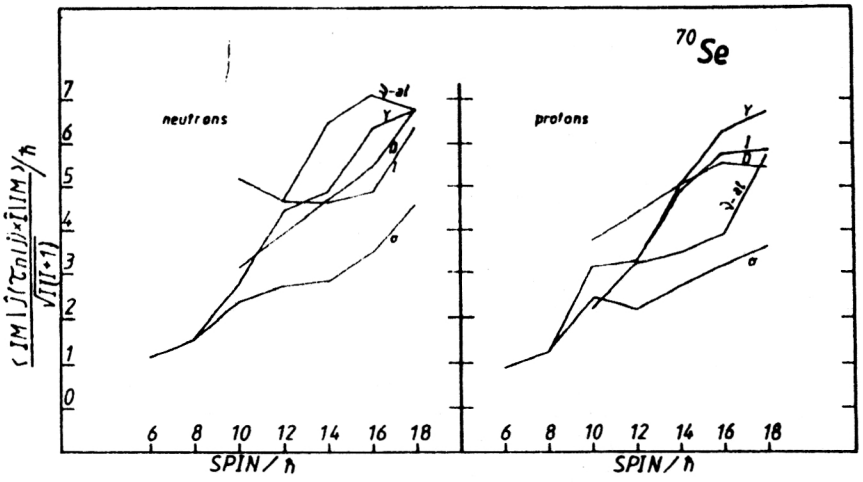

FIG. 15. The neutron and proton alignments of the $0g_{9/2}$ orbit, as in the bottom part of Fig. 13, but for the nucleus ^{70}Se studied in the REV approximation.

$B(E2)$ values, become strongly mixed and follow essentially the same decay path. Both the 14_2^+ and the 14_3^+ level feed, via $M1$ transitions, the yrast 14_1^+ level and, via $B(E2)$ transitions, subsequently the 12_3^+ and 10_3^+ levels. These in turn decay via strong $M1$ transitions with $B(M1;12_3^+ \rightarrow 12_1^+) = 2.01\mu_N^2$ and $B(M1;10_3^+ \rightarrow 10_1^+) = 2.21\mu_N^2$ into the yrast level, and because of the strong mixing of the lowest two 10^+ states a considerable value $B(M1;10_3^+ \rightarrow 10_2^+) = 1.32\mu_N^2$ leads to the oblate band too. The two lowest 10^+ states then both decay preferentially into the oblate 8_1^+ configuration. The last of the above-mentioned four bands consists of the yrast levels above spin 12^+. The band labeled *Y* displays $B(E2)$ values comparable to those obtained for the *O*, the *ν–al*, and the *I* band. However, because of a rather small energy splitting within this band, especially between its 16_1^+ and 14_1^+ members, the corresponding decay path is relatively slow. We should mention here that the strongly deformed high-spin band found in the ^{68}Ge nucleus has no counterpart in the ^{70}Se nucleus, at least in the present *real* EXCITED VAMPIR description. Obviously, it cannot be excluded that such a band may be found at higher excitation energy in this nucleus too.

It is worth mentioning that strong magnetic dipole transitions linking the various bands with each other in the intermediate spin region are obtained in the ^{70}Se nucleus too. As expected in this spin region, a competition of several configurations resulting from the various possible couplings of the $0g_{9/2}$ valence protons and neutrons is revealed by the structure of the wave functions, and in most cases the strong $B(M1)$ values are dominated by amplitudes corresponding to the reordering of nucleons in this shell-model orbit. As a consequence, these transitions usually contain considerable (about 50%) orbital components.

Finally, a few words concerning the comparison with the experimental data[35,36] presented in the right part of Fig. 9. Up to angular momentum 8^+ we obviously have to identify the theoretical yrast states with the experimental ones. In this spin region the transition energies are in fair agreement, as are the values of $B(E2;2_1^+ \rightarrow 0_1^+)$. On the other hand, the experimental $B(E2)$ values for $6_1^+ \rightarrow 4_1^+$ and $4_1^+ \rightarrow 2_1^+$ are considerably smaller than those predicted theoretically. Here the inclusion of additional correlations within the EXCITED FED VAMPIR approach may help, as well as a renormalization of the effective Hamiltonian, which seems to be necessary, as will be discussed later in

TABLE II. The spectroscopic quadrupole moments Q_2^{sp} ($e \cdot \mathrm{fm}^2$) for some of the REV bands obtained for the nucleus ^{70}Se and displayed in Fig. 9. As effective charges, again the same values as in ^{68}Ge have been taken. The labels (*O,Y,D,I,ν–al*) referring to the various bands are explained in the text.

$I[\hbar]$	*O*	*Y*	*D*	*I*		*ν–al*
2	43					
4	61					
6	68					
8	69					
10	20	−26	−101		−78	
12	56	−75	−98		−70	
14	66	−77	−100	−81		−83
16	63	−79	−99	−80		−78
18	59	−79	−84	−81		−84

the context of these calculations. However, it cannot be excluded that the uncertainties in the feeding times[4] may lead to changes of the experimental data too. Here, obviously, more information is needed before definite conclusions can be drawn. The same holds for the classification of the experimental levels above angular momentum 8^+. Here the present calculations offer three candidates: the oblate band, displaying the fastest decay, but having a somewhat too small moment of intertia in this spin region, the deformed band *D*, or the neutron-aligned band. These last two structures reproduce the experimental transition energies quite nicely; however, both imply a previously unobserved strong magnetic dipole transition. Thus, the present investigation can only be considered as a first guide to the nucleus ^{70}Se, and many more theoretical and experimental studies seem to be required before a satisfactory understanding is reached.

In order to obtain some more information about the systematic trends and variations in this mass region we investigated the low- and high-spin states of the nucleus ^{72}Se with two extra neutrons with respect to ^{70}Se and two neutrons and two protons more than ^{68}Ge. Again, the same model space and effective Hamiltonian as for ^{68}Ge and ^{70}Se were used within the *real* EXCITED VAMPIR approximation.

In ^{72}Se the experimentally observed gamma rays are linked in a single positive-parity band up to spin 28^+ (Refs. 17 and 36). All crossing transitions to other side bands observed up to now have experimental branching intensities less than 10% of the observed cascade feedings. In the ^{72}Se nucleus we analyzed all the possible decay paths starting from the first six 22^+ states. Of course, only positive-parity even spin states have been investigated. Again, the prolate–oblate coexistence dominates the structure of the low- and high-spin states in ^{72}Se. For the low-spin yrast states a dominant oblate character emerges from the structure of the wave functions and the spectroscopic quadrupole moments for 2_1^+ and 4_1^+ states. The strongest prolate–oblate mixing appears for the 6_1^+ and 6_2^+ states. This strong mixing makes a small quadrupole moment for the 6_1^+ state. The first predominant oblate state of the band labeled (*o*) in Fig. 10 is the 8_2^+, and so are all the higher spin states belonging to this band. The intrinsic quadrupole deformation of the oblate mean fields underlying the structure of these oblate band states varies very slowly and smoothly to smaller Q_2 values with increasing spin. The oblate band could be characterized as a vibrational band, with almost equidistant levels and nearly constant spectroscopic quadrupole moments. These $Q_2^s(I)$ are small compared with those of all the other analyzed bands, and the $B(E2)$ values are almost constant around 50 W.u. All the other bands presented in Fig. 10 are prolate deformed bands, as is illustrated by the spectroscopic quadrupole moments for these states given in Table III. Again, effective charges of 0.25 for the neutrons and 1.25 for the protons were used. The large range of REV $B(E2)$ values (Table III) characterizing the intraband $E2$ transitions reflects the different quadrupole deformations.

Classifying the states in bands solely on the basis of the $B(E2)$ values, we tried to find the fastest ways to enter the yrast line. The fastest prolate decaying paths are pointed out in Fig. 10. However, a detailed look at the calculations reveals that there is a path of very fast cascade $E2$ transitions which cross from one band to another with the largest (*S—strong*) quadrupole deformation with only slow (weak) transitions to other states. Thus, it is possible that the experimental yrast band seen to high spins is a composite of several bands, all with quite large deformation and linked by a very fast $E2$ path. In Table III we give for comparison the experimental $B(E2)$ values reported by different groups.[40,45,46] The experimental trend observed in the $B(E2)$ values could be reproduced by a theoretical composite path consisting of high spins from the *S*-band states which feeds, by strong $M1$, $\Delta I=0$ transition, the yrast band at spin 10^+. Large $B(E2)$ values above spin 10 also indicate the oblate band as a possible competing band. One needs more lifetime measurements to test this prediction.

The analysis of the wave functions reveals a variable mixing of more or less deformed prolate mean fields. The fastest decaying bands are strongly deformed quadrupole bands (labeled *S* and *D* in Fig. 10). Again, strong $M1$, $\Delta I=0$ transitions connecting medium spin states have been found.

Figure 16 displays the neutron and proton alignments for the $g_{9/2}$ spherical orbital in the above labeled bands. No sharp alignment can be seen. This microscopic picture explains the missing backbending inferred from the experimental spectrum of ^{72}Se. The neutrons and protons bring almost the same contributions to the total angular momentum in all bands except for the oblate band, where the alignment for the two protons is, as expected, more difficult. In the upper part of Fig. 16 we show for comparison the occupation numbers for protons and neutrons in the $g_{9/2}$ spherical orbit.

The alignment picture is directly reflected by the gyromagnetic factors given in Fig. 17 for the *a*, *S*, *I*, *D* and oblate bands. Small *g* factors characterize only the oblate states, as is suggested by the strong neutron and weak proton alignment displayed in Fig. 16. Thus, the *g*-factor values could be used in this case as a possible fingerprint of the oblate band. Free values for the neutron and proton spin *g* factors were used throughout the calculations.

Since the experimental information on the high-spin states is far from complete and the accuracy of the data is still rather poor, we think that our theoretical results and also the conclusions emerging from the calculations of the side feeding times in this mass region[40] raise many questions and would justify the continuation of the experimental investigations of the nucleus ^{72}Se.

3.3. Discussion

Summarizing the results obtained within the *real* EXCITED VAMPIR approximation concerning the structure of the positive-parity low- and high-spin states of even–even nuclei in the $A\sim 70$ mass region, we may conclude that many types of shape coexistence have been found. Our interpretation strongly supports the shape coexistence as a

TABLE III. REV spectroscopic quadrupole moments and $B(E2;I\to I-2)$ values for the states belonging to the specified (o,a,S,I,D) bands of the nucleus ^{72}Se. The available experimental results are given for comparison (Refs. 40, 45, and 46). The labels of the bands are the same as in Fig. 10. The effective charges were $e_n=0.25$ and $e_p=1.25$.

$I[\hbar]$	$Q_2^{sp}[e\cdot\mathrm{fm}^2]$							
	o	a	S	I	D			
2	34							
4	47							
6	−37	18						
8	67	−87	−96		−95			
10	76	−91	−99		−93			
12	73	−86	−107		−104			
14	76	−83	−111		−105			
16	76	−83	−113		−95 −97			
18	73	−83	−106	−81	−103			
20	49	−83	−110	−83	−81			
22	66	−83	−107	−85	−96			
$I[\hbar]$	$B(E2;I\to I-2)\ [e^2\mathrm{fm}^4]$							
	Theory					ref.[45]	ref.[46]	ref.[40]
2		627				400±50	356±36	427±53
4		996				1060±160	801±107	1085±160
6		1100				900±90	1068±178	907±71
8	734	869				1250±150	1263±142	1263^{+178}_{-142}
10	1067	1407				1510±180	1744±231	1512^{+231}_{-178}
12	1118	910	1371		1191		1637±178	1619^{+409}_{-267}
14	1044	920	1987		1606		2544^{+2544}_{-854}	2491^{+1495}_{-676}
16	1180	1062	1923		880 710			
18	1132	701	1599		563 999			
20	1028	868	1157	501	1326			
22	928	858	1644	746	1103			

dominant feature of the low-spin states. This persists and manifests itself specifically for high-spin states. We predicted a strong bunching of states of a given spin in a small excitation energy interval and a variable, sometimes very strong, mixing between these states, which creates a complex feeding pattern for the yrast band, including competing $M1$, $\Delta I=0$ transitions. Nevertheless, the high-spin states can still be grouped into multiple bands based on different structures, some of them connected by $E2$ crossing transitions.

This complex behavior was provided by an approximation which, at least in principle, can describe excitations of arbitrary complexity, and by its chain of variational calculation automatically selects the relevant degrees of freedom for each particular state under consideration, irrespective of whether they are of collective or single-particle nature. Furthermore, by construction this approach minimizes the residual interaction between its different solutions and hence successively creates an optimal A-nucleon basis for a given symmetry. Thus, it is expected that already with a small number of configurations an excellent description of the structure of the investigated states can be reached.

Now, concerning the comparison of our results for the $A\sim 70$ mass region with the experimental information, qualitatively the overall agreement with the available data is not bad; quantitatively, however, especially as far as the $B(E2)$ values are concerned, there are still many discrepancies and open problems. Since experimentally the side feeding times in this mass region are not yet firmly handled,[40] the measured $B(E2)$ values reported by different groups are too strongly spread and the available data concerning other observables are too scarce, we saw no reason to change the renormalization of the effective Hamiltonian. Obviously, changes in this renormalization as well as the inclusion of additional correlations were supposed to alter the quantitative results obtained within the *real* EXCITED VAMPIR approximation. However, with regard to the qualitative features such as the coexistence of many differently deformed structures and the resulting high level density even for the high-spin values, one would expect these to survive after such improvements of the theoretical description. What we have obtained by pro-

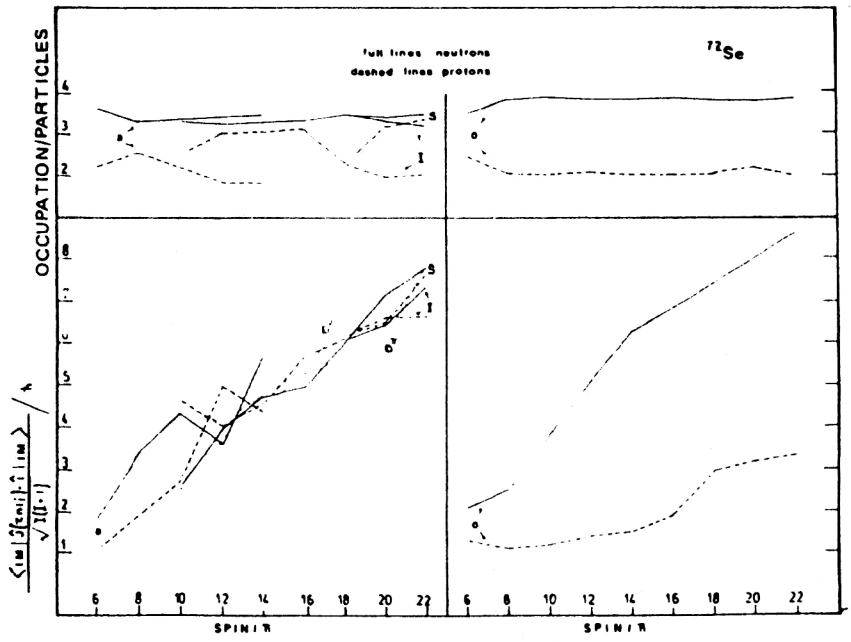

FIG. 16. The same as in Fig. 13, but for ^{72}Se, using again full lines for neutrons and dashed lines for protons. The labels of the bands are the same as in Fig. 10.

ceeding on these lines to get improvements and tests of our achievements will be described in the next section.

4. NEW ASPECTS OF THE NUCLEAR-SHAPE COEXISTENCE VIA THE *REAL* EXCITED FED VAMPIR APPROACH

Being restricted always to only one additional determinant for each new state with the considered symmetry, the EXCITED VAMPIR approach is, however, essentially a mean-field approximation. The residual interaction between the lowest few configurations for each symmetry may not be the dominant one for the lowest states, especially in regions with a high level density, as is encountered in the $A \sim 70$ mass region. The EXCITED FED VAMPIR approximation, which allows one to include the dominant correlations for each particular configuration irrespective of their excitation energy in a systematic way, using again variational procedures, has the advantage that the residual interaction between the correlated states becomes much smaller than in the case of the uncorrelated EXCITED VAMPIR solutions and thus increases the reliability of the wave functions considerably. In the following we shall demonstrate that the qualitative features of the complex behavior of the nuclei in the $A \sim 70$ region obtained within

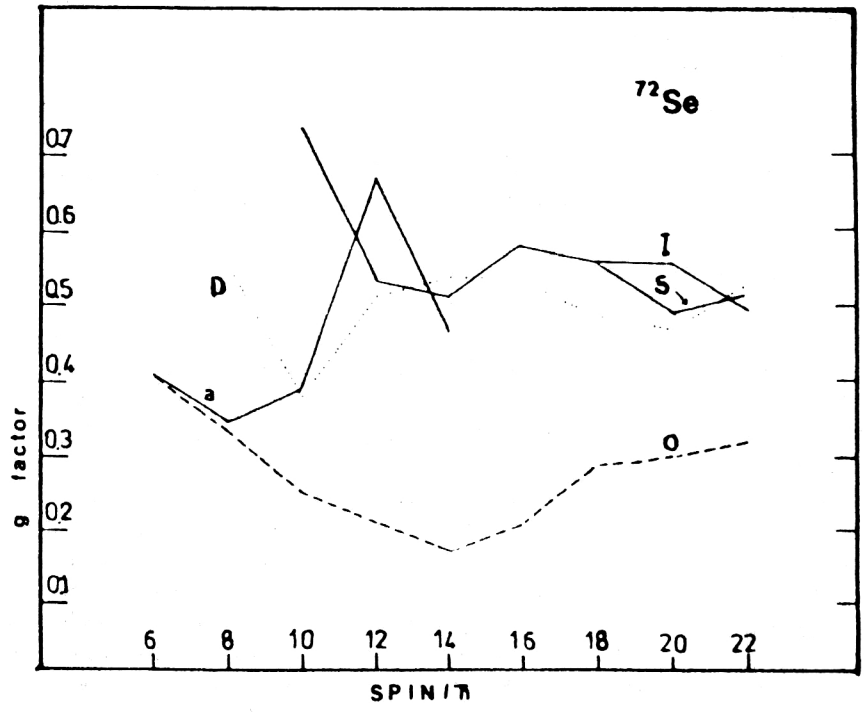

FIG. 17. The same as in Fig. 14, but for ^{72}Se.

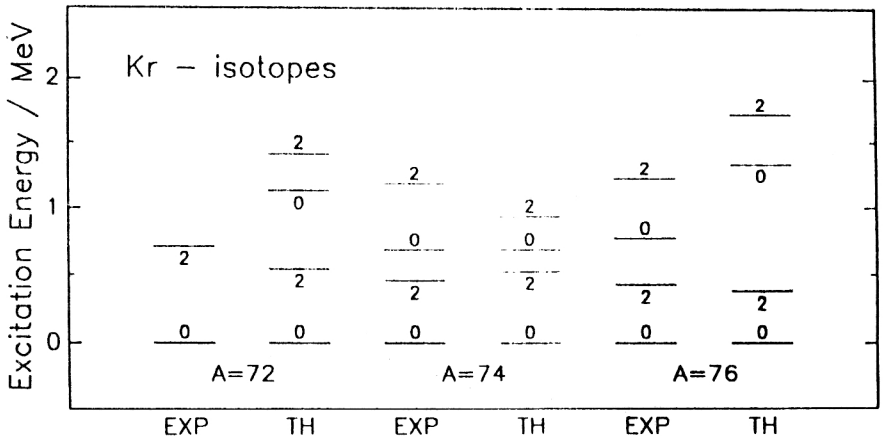

FIG. 18. The excitation energies of the first excited 0^+ states as well as of the lowest 2^+ states, obtained within the *real* EXCITED FED VAMPIR approach for the isotopes[72,74,76]Kr, compared with the experimental data.

the less sophisticated EXCITED VAMPIR procedure persist; however, quantitatively new aspects could be obtained.

4.1. Charge and transition charge densities in some even-mass Ge isotopes

Based on the assumptions given in Sec. 2.1, the effective Hamiltonian for all the considered nuclei was built as explained in Sec. 3.1. Then correlated *real* EXCITED FED VAMPIR wave functions for the lowest two $I^\pi=0^+$ and 2^+ states were calculated in two chains of isotopes: [68,70,72,74,76]Ge and [72,74,76]Kr. As described above, for each particular state, first a single symmetry-projected configuration, being properly orthonormalized with respect to the correlated solutions for the energetically lower states with the same symmetry, was used as a trial wave function. The resulting "dominant mean-field configuration" was then correlated by successively adding further determinants and determining the underlying mean fields again by variation. In this procedure the energy gains due to subsequently added configurations decrease by construction, and the chain of variational calculations was truncated as soon as these gains became of the order of about 100 keV. The resulting numbers of symmetry-projected quasiparticle determinants used for each state varied from 4 to 6 for the 0^+ ground states and from 4 to 5 for the first excited 0^+ levels. For angular momentum 2^+ the corresponding numbers were 3 to 5 for the first and 2 to 4 for the second state, respectively. Finally, the residual interaction between the correlated solutions for the same symmetry was diagonalized.

A picture similar to the *real* EXCITED VAMPIR one emerged from the *real* EXCITED FED VAMPIR studies on the structure of low-spin states in the investigated chains of Kr and Ge isotopes. In Fig. 18 the excitation energies for the calculated $I^\pi=0^+$ and 2^+ states in the [72,74,76]Kr nuclei are compared with the available experimental data. As can be seen, the agreement is fairly good, especially for a completely microscopic calculation. The structure of the lowest two 0^+ and 2^+ states in the Kr isotopes is dominated by oblate–prolate shape coexistence.

In a next step we tried to confirm a rather complicated picture emerging from the REV and REFV approaches for the structure of nuclei in the $A\sim 70$ mass region on a more quantitative basis. For this purpose we calculated the charge densities for the first two $I^\pi=2^+$ states in several even Ge isotopes[18] and compared the results with the data extracted from elastic and inelastic electron scattering.[19]

The wave functions resulting from any of the approaches presented in section 2.2 are quantum-mechanical many-particle states having proper symmetry quantum numbers and can thus be used to calculate various observables. In order to obtain the transition charge density between two REFV solutions $|\Psi_i\rangle$ and $|\Psi_f\rangle$ for a particular nucleus, e.g., we have to calculate the matrix elements of the charge-density operator

$$\hat{\rho}_{ch}(\mathbf{r})=\frac{1}{(2\pi)^3}\int d^3\mathbf{q}\,\exp\{i\mathbf{q}\cdot\mathbf{r}\}f_{CM}(q)f_p(q)\times\sum_{i=1}^{A}e_{\tau_i}\exp\{-i\mathbf{q}\cdot\mathbf{r}_i\} \tag{4.1}$$

between these two states. Here e_{τ_i} denotes the effective charge of the proton or neutron i, and the Gaussian

$$f_p\equiv\exp\left\{-\left(\frac{aq}{2}\right)^2\right\} \tag{4.2}$$

with a width parameter $a=0.656$ fm approximates the charge distribution of a single proton.[47] The usual Tassie–Barker factor[48]

$$f_{CM}\equiv\exp\left\{\frac{1}{A}\left(\frac{bq}{2}\right)^2\right\} \tag{4.3}$$

was introduced to correct the violation of the translational invariance in both the operators and the wave functions (b is the oscillator length parameter used for the single-particle basis wave functions). This correction factor is completely sufficient here for the approximate treatment of the center-of-mass motion, because of the relatively large mass of the nuclei considered, and since, furthermore, a pure harmonic-oscillator single-particle basis is used.

The theoretical description of the spectra and electromagnetic transition probabilities which were illustrated above is also supported by the results[18] for the charge transition densities from the ground to the first and second 2^+

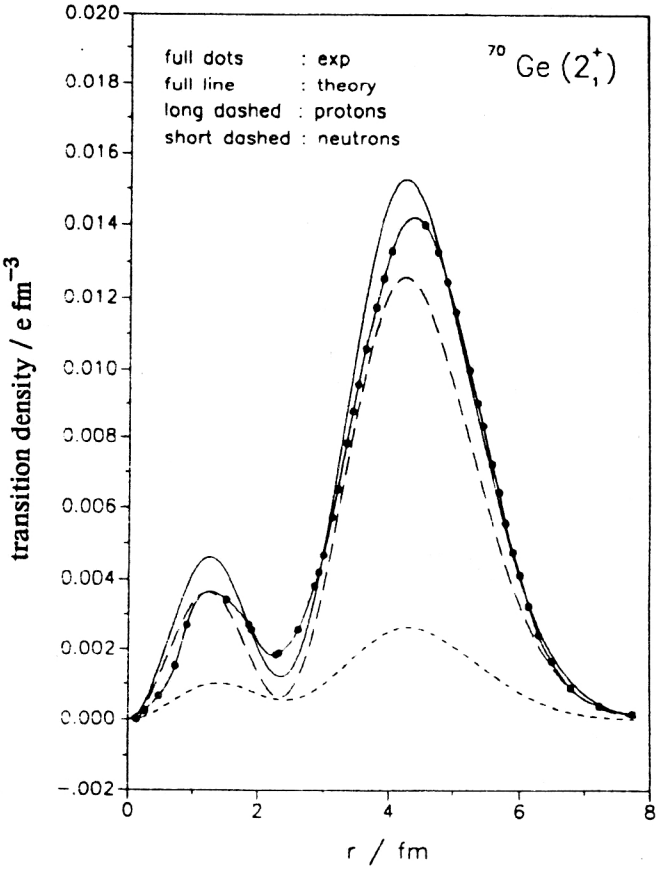

FIG. 19. The calculated transition charge density for the 2_1^+ state in ^{70}Ge, compared with the experimental data of Ref. 19. The total theoretical transition density is furthermore decomposed into its proton and neutron components. Effective charges $e_n=0.17$ and $e_p=1.17$ have been used.

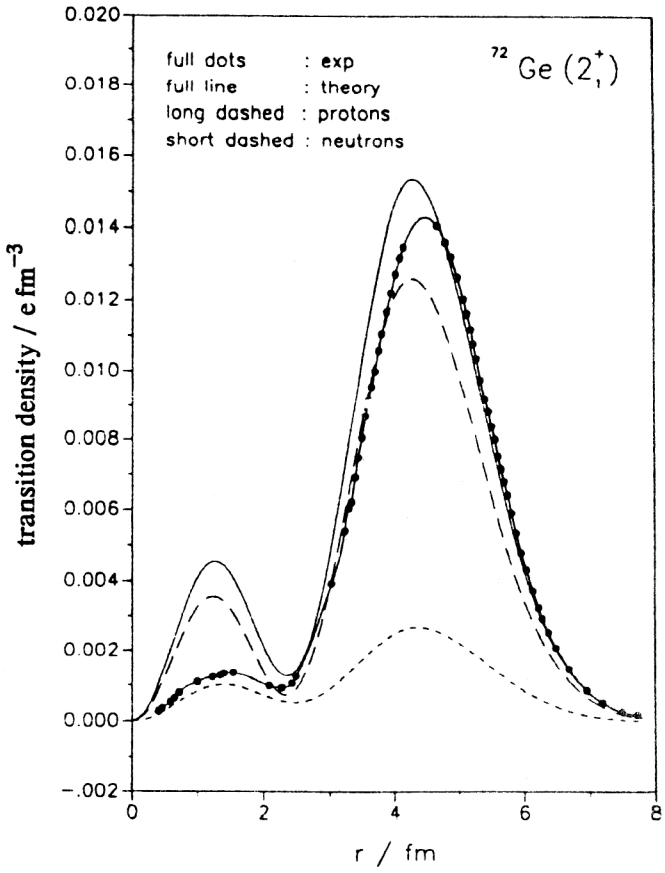

FIG. 20. The same as in Fig. 19, but for the 2_1^+ state in ^{72}Ge.

levels in several Ge isotopes. As an example, we compare the calculated charge transition density to the collective 2_1^+ state in ^{70}Ge and ^{72}Ge with the experimental results[19] from inelastic electron scattering in Figs. 19 and 20, respectively. As can be seen, the agreement is excellent. For ^{74}Ge and ^{76}Ge, however, the magnitude of the experimental transition density is considerably understimated, though the shape is in both cases reasonably well reproduced by the calculations. It should be mentioned that here no adjustment of the effective charges (0.17 for neutrons and 1.17 for protons) used in the REFV calculations to investigate other electromagnetic properties of the considered nuclei has been made. The transition charge densities for the much smaller noncollective transitions to the second 2^+ states are obviously even more sensitive. However, here too, the shapes of the calculated densities are in reasonable agreement with experiment (with the exception of the small negative hump at small radii in ^{74}Ge), and the magnitude of the densities can also be reproduced, as can be seen from Figs. 21 and 22. In these figures the transition charge densities obtained for the noncollective 2_2^+ transitions in ^{72}Ge and ^{74}Ge, respectively, are compared with the available experimental data. In ^{76}Ge again the shape of the experimental transition charge density is reasonably well reproduced, while the magnitude is drastically underestimated.

Both the 2_1^+ and the 2_2^+ transitions are better reproduced in the present calculations than in the Skyrme–Hartree–Fock–Bogolyubov calculations of Girod, Gogny, and Grammaticos,[49] discussed also in Ref. 19. The improvement obtained by the present symmetry-projected few-determinant calculations over the one-determinant Skyrme–HFB description is a strong indication that the mixing of configurations corresponding to different shapes, which is obtained as the prominent feature of the structure of the low-spin states of the nuclei in this mass region in our completely microscopic variational calculations, does play an important role, at least in the doubly even Ge, Se, and Kr isotopes.

4.2. Some new aspects of the shape coexistence in the nucleus ^{68}Ge

Using the same model space and the same effective Hamiltonian as in the *real* EXCITED VAMPIR approximation, we reinvestigated the spectrum of ^{68}Ge with the *real* EXCITED FED VAMPIR procedure, not without some hesitation, since our earlier more restricted description of this nucleus got at least some qualitative support from new experimental data.[17] Fortunately, however, as we shall see, the qualitative features of the earlier description are retained.

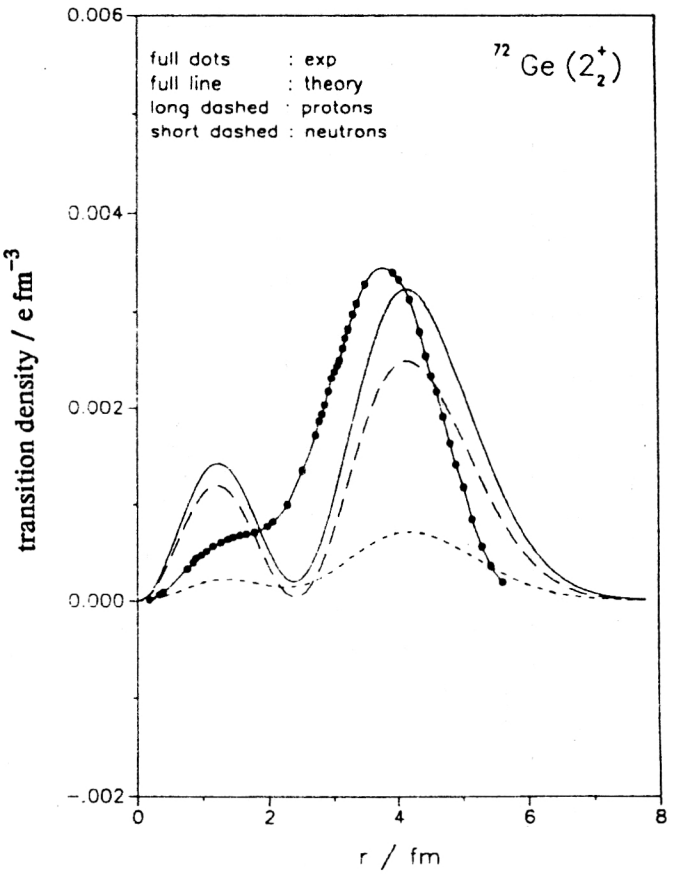

FIG. 21. The same as in Fig. 19, but for the 2_2^+ state in ^{72}Ge.

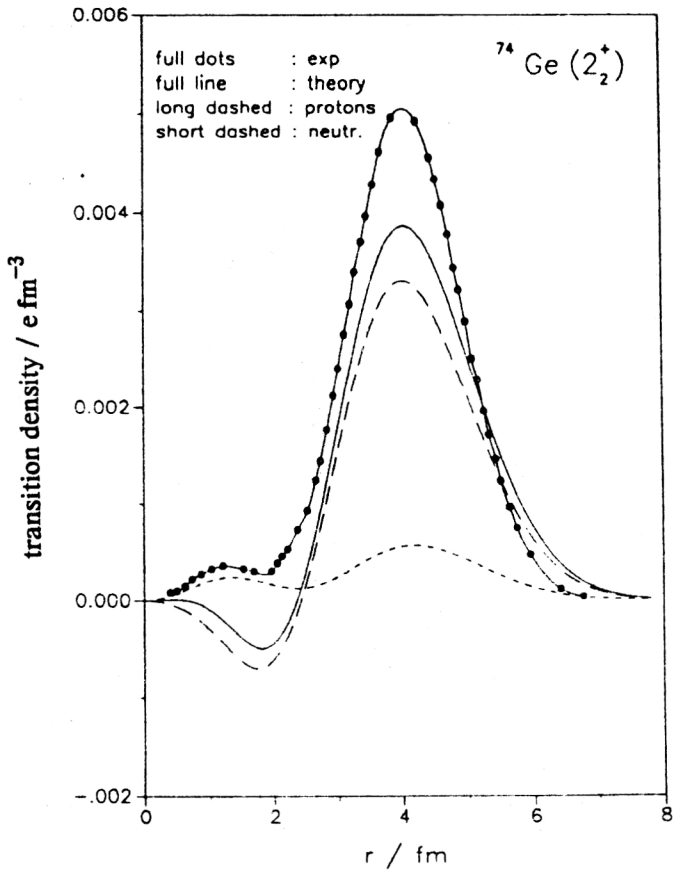

FIG. 22. The same as in Fig. 19, but for the 2_2^+ state in ^{74}Ge.

We have constructed correlated REFV wave functions for the three lowest 0^+, 2^+, and 4^+, the four lowest 6^+, the five lowest 8^+, 10^+, 12^+, and 14^+, the six lowest 16^+, and the seven lowest 18^+ levels of ^{68}Ge. As was already mentioned, first the "main mean field" is obtained, and then the "correlating configurations" for each state of a given symmetry. The additional correlations have been kept in the variational chain as long as the energy gain was still of the order of 100 keV. The resulting numbers of symmetry-projected quasiparticle determinants used for each state varied from 1 to 7. After the diagonalization of the residual interaction, here much smaller than in the REV approach, the solutions were grouped into several bands entirely according to the $B(E2)$ transitions between them. The new theoretical spectrum together with the new experimental results are given in Fig. 23. Since neither the model space nor the effective interaction was changed, the results can be compared directly with what was obtained within the more restricted EXCITED VAMPIR approach.

In comparing the EXCITED FED VAMPIR spectrum (left side of Fig. 23) with the EXCITED VAMPIR one (left side of Fig. 8) it becomes obvious that the essential qualitative features of the calculated spectrum, like the occurrence of many coexisting bands at comparable excitation energies and the complexity of the resulting decay pattern, are not influenced by the additional correlations. Furthermore, all the various bands obtained in the earlier calculations also occur in the improved approach. This can be seen, e.g., from Table V, in which we compare the spectroscopic quadrupole moments and $B(E2)$ values of these bands as obtained in the REFV approach with those resulting from the REV uncorrelated calculations. Except for some discrepancies at angular momentum 8^+ and 14^+, the agreement is very good. Furthermore, the fact that in both calculations essentially the same structures are obtained is supported by the amount of angular momentum which the valence protons and neutrons in the $0g_{9/2}$ shell-model orbit contribute to the total spin in various bands. A comparison of the alignment plots is given in Fig. 24. As can be seen, the inclusion of the additional correlations by REFV again causes no essential qualitative modifications with respect to the REV results. Since, last but not least, also the transition energies within various bands were in most cases not very much affected, we may conclude that, at least as far as the qualitative features are concerned, our REV description of this nucleus was essentially confirmed by the more sophisticated REFV procedure.

In their quantitative details, however, the two approaches display some distinct differences. Comparing, e.g., the energy of the correlated few-determinant solution (before the diagonalization of the residual interaction) with that of the dominant first configuration, being created for each state, one obtains in most cases energy gains which are comparable with the level spacings and thus considerable. Table IV displays these "correlation energies" as well as the corresponding deviations of the corre-

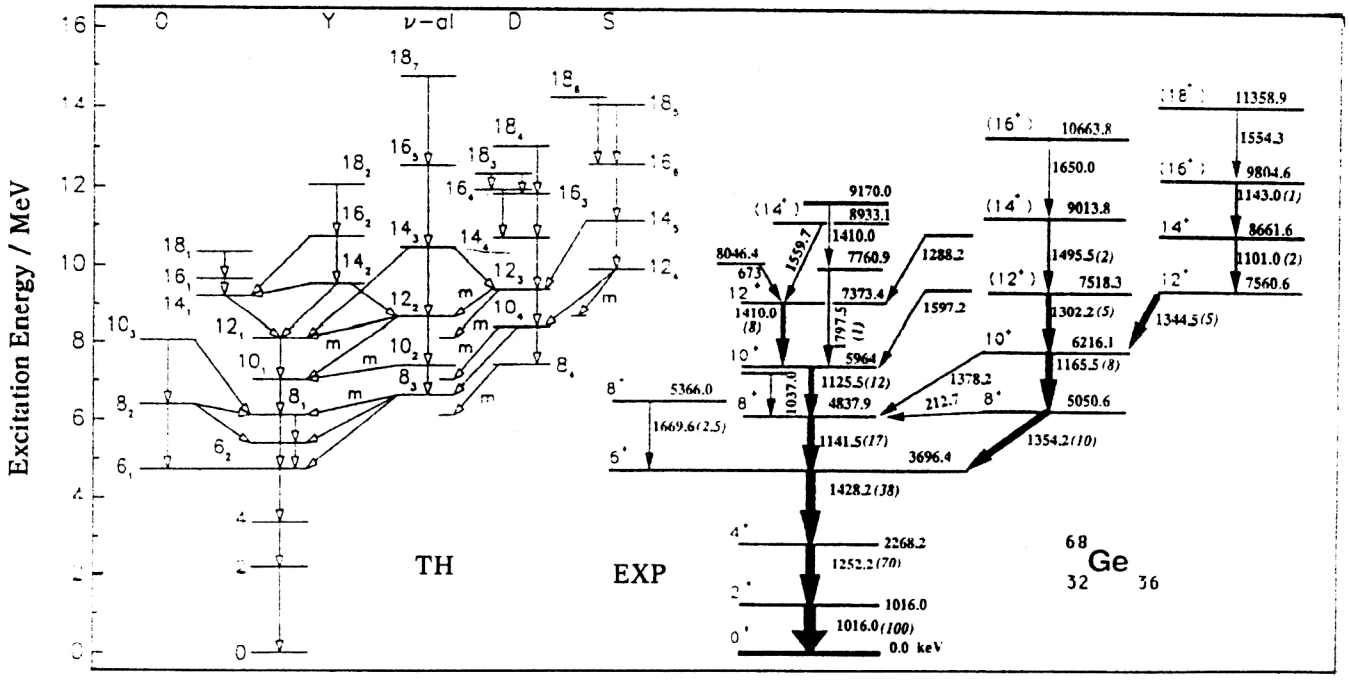

FIG. 23. Positive-parity levels in the ^{68}Ge nucleus. The theoretical spectrum as obtained in the *real* EXCITED FED VAMPIR approach (left side), compared with recent experimental results (right side). The symbols used to identify the calculated bands are described in the text. The experimental bands are ordered (oblate on the left, superdeformed on the right) to match with the calculated levels on the left side and to match the observed properties (lifetimes, magnetic moments, and moments of inertia) of each band with the calculated properties of each band. The *D* band in the calculations may be the new band which feeds the 5963-keV 10^+ level (Ref. 17).

lated solution from the dominant "one-configuration" wave functions for a number of selected states. As can be seen, the correlation energies, which are on the average of the order of about half a MeV, display, however, some variations with angular momentum as well as excitation energy. The corresponding deviations from the dominant component in the wave function vary from almost nothing to about 30%. Note that the states selected here are typical examples. For all the other levels of Fig. 23 similar results have been found.

The most drastic effect is obtained for the 0^+ ground state: altogether about 6% of the correlations, but 1221 keV of additional binding for the REFV solution, which is about half a MeV more than any energy gain found for the higher spin states. Consequently, the $2_1^+ \rightarrow 0_1^+$ transition energy now becomes considerably larger than that ob-

TABLE IV. The size of the correlations and the corresponding energy gains obtained within the *real* EXCITED FED VAMPIR approach for some selected states of the nucleus ^{68}Ge *before* the residual interaction between the various solutions for each considered symmetry is diagonalized.

I_i [ħ]	n_c	$\lvert\psi_c\rvert^2$ [%]	E_c [keV]	I_i [ħ]	n_c	$\lvert\psi_c\rvert^2$ [%]	E_c [keV]
0_1	4	6	1221	12_1	4	27	681
2_1	6	14	637	12_2	3	14	409
2_2	4	14	502	16_1	3	14	685
2_3	2	20	708	16_2	4	14	842
8_1	2	2	226	18_1	3	9	596
8_2	4	12	502	18_2	2	17	668
8_3	5	24	767	18_3	1	14	605
10_1	4	16	550				
10_2	4	8	521				
10_3	2	4	274				

The first column presents the angular momentum with a subscript referring to the position of the state in the spectrum. In the next column the number of correlating configurations being used on top of the dominant mean field configuration for this particular state is presented. The amount of correlations $\lvert\psi_c\rvert^2$ they contribute with respect to the latter is given in the next column and, finally, the corresponding correlation energy is presented. Note that this numbers refer to the already *orthonormalized* solutions

TABLE V. The spectroscopic quadrupole moments Q_2^{sp} (in $e \cdot \mathrm{fm}^2$) and $B(E2;I \to I-2)$ values (in $e^2\mathrm{fm}^4$) for some of the theoretical bands obtained for the nucleus ^{68}Ge.

	Q_2^{sp} [$e \cdot \mathrm{fm}^2$]							
I[ħ]	Y		$\nu - al$		D		S	
	REFV	REV	REFV	REV	REFV	REV	REFV	REV
2	28	29						
4	49	48						
6	55	53	−72	−68				
8	−56	−40	−62	−71	−102	−87	−102	−77
10	−75	−79	−65	−59	−107	−106	−107	−102
12	−81	−78	−66	−68	−92	−103	−108	−99
14	−83	−85	−53	−54	−98	−104	−120	−110
16	−86	−86	−53	−55	−97	−96	−118	−117
18	−85	−89	−45	−46	−96	−93	−103	−101

	$B(E2; I \to I-2)$ [$e^2\mathrm{fm}^4$]							
I[ħ]	Y		$\nu - al$		D		S	
	REFV	REV	REFV	REV	REFV	REV	REFV	REV
2	100	181						
4	563	633						
6	792	834						
8	291	503						
10	852	798	677	500	1870	1367		
12	854	919	619	561	1234	1259	733	1549
14	273	332	285	206	856	1207	1732	1449
16	672	960	388	349	1137	997	2163	1390
18	921	907	325	237	837	708	1445	1148

Compared are the results of the *real* EXCITED FED VAMPIR (REFV) calculations (Fig.23) and those of the more restricted *real* EXCITED VAMPIR (REV) approach (Fig.8). In both cases effective charges of $e_n = 0.25$ and $e_p = 1.25$ have been used. The labels referring to various bands are explained in the text

served experimentally. There are essentially two reasons for this discrepancy. First, to make a comparison of REV and REFV results we used the renormalizing corrections to the nuclear-matter G matrix, adjusted within the EXCITED VAMPIR approximation and not within the more general few-determinant approach. Second, even in the REFV approximation the underlying mean fields are still considerably "symmetry-restricted," and we shall see in the next section what improvement the introduction of a "complex" HFB mean field gives. Keeping this deficiency in mind, we shall compare the REFV results with the new experimental data[17] for the high-spin positive-parity bands in the nucleus ^{68}Ge by renormalizing the theoretical spectrum to the corresponding 2_1^+ level.

Up to angular momentum 6^+ the calculated yrast levels are almost pure oblate states. The oblate band (O in Fig. 23) then continues with the second 8^+ (about 85% oblate), which probably has to be associated with the experimental 8_3^+, and, as in the REV approximation, starting with 10_3^+ these oblate states are almost pure, but at rather high excitation energy, and therefore probably only weakly populated. Besides this oblate structure, four other pronounced bands are obtained in the calculations. They are all prolate-deformed but differ in the magnitude of their quadrupole and hexadecapole moments as well as in their pairing properties and display different alignments too.

As in REV calculations, the band labeled ν–al is characterized by an almost empty $0g_{9/2}$ proton level, while the neutrons in the same shell-model orbit contribute here a considerable portion of the total angular momentum. This strong neutron alignment is reflected in the small g factors of the members of this band, again with a small negative value for the 8_3^+, as in the REV approach and in the data for the experimental 8_2^+.

The two bands labeled D and S have almost the same quadrupole deformation on the neutron side; however, on the proton side the latter band is considerably more deformed. This is evident from the intrinsic quadrupole moments ($\beta_2 \cong 0.42$ as compared with $\cong 0.34$) of the leading configuration as well as from the $B(E2)$ values, which above spin 12^+ are about twice as large in the S as in the D band. It should be stressed that in the recent experimental data one of the new bands has a larger moment of inertia than the previously known ones. In fact, as can be seen by comparing the old data (Fig. 8) and the new ones (Fig. 23), the three known bands beginning at 8^+ are found to exibit crossing transitions, and other new bands are discovered to feed into them. It is remarkable that the complex band structure predicted by the calculations (REV as well as REFV) is supported by a similar picture revealed by the new experimental evidence.

All the calculated prolate bands have one common feature: their members become strongly mixed as soon as spin values as low as 14^+ or 12^+ are reached. Consequently, there are many competing decay branches for the various 14^+, 12^+, 10^+, and even 8^+ states. Thus, the decay runs not only via stretched $E2$'s within the various bands but also via some rather strong $B(E2)$'s for $\Delta I = 2$

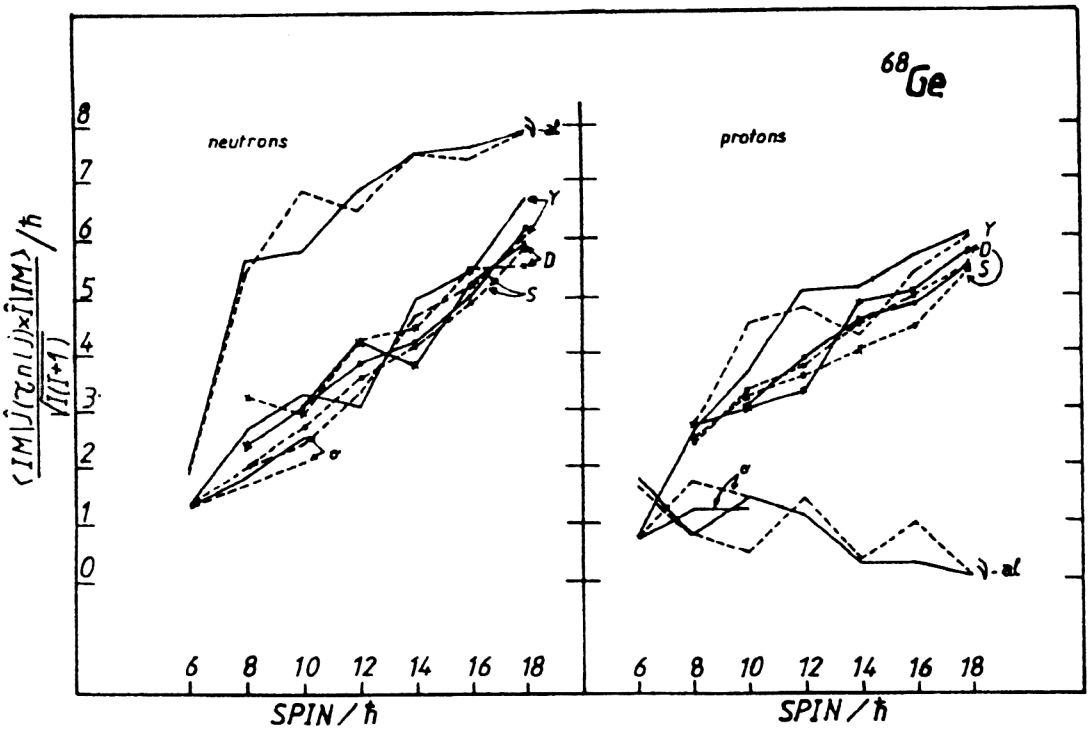

FIG. 24. The neutron (left side) and proton (right side) alignments of the $0g_{9/2}$ shell-model orbit for the nucleus ^{68}Ge. The full lines refer to the results of the correlated *real* EXCITED FED VAMPIR approach; the dashed ones, to those of the more restricted *real* EXCITED VAMPIR calculations.

as well as a number of strong $\Delta I=0$, $M1$ transitions (indicated by m in the figure), mainly feeding the yrast band (Y) at these angular momenta. Thus, e.g., the calculated 8_1^+ is linked to the 8_3^+ and the 8_4^+ by $B(M1)$ values of 1.94 and 0.46, the 10_1^+ to the 10_2^+ and the 10_4^+ by even 4.21 and 0.47, and the 12_1^+ to the 12_2^+ and 12_3^+ by 0.82 and 0.64 (all in μ_N^2), respectively. Such crossing transitions are also seen in the new experimental data. The resulting complex decay pattern may explain at least some of the irregularities seen in the experimental data, and obviously the theoretical results are strongly supported by the observation of not only several 8^+ but also several energetically bunched 10^+, 12^+, and 14^+ states.

With regard to the $B(E2)$ values, it is expected that uncertainties in the feeding times in such complex decay patterns as are observed in the ^{68}Ge nucleus could lead to considerable errors, and this may be the reason for the large error bars and the disagreement in the data from several experiments.[34,37–39] Thus, the comparison with the data needs a lot of further investigation. As can be seen from Table V, the EXCITED FED VAMPIR approach yields for the $B(E2)$ values results rather similar to those of the more restricted EXCITED VAMPIR approximation; thus, in this respect the inclusion of the additional correlations yields no new aspects.

4.3. Discussion

We have tried to test our microscopic description of the complex behavior of the nuclei belonging to the $A\sim 70$ mass region using the more sophisticated *real* EXCITED FED VAMPIR approach. These studies confirmed a rather complicated picture emerging from the *real* EXCITED VAMPIR approximation for the considered nuclei.

Increasing the reliability of the resulting wave functions considerably by introducing additional correlations on the top of the symmetry-projected quasiparticle mean fields, we reinvestigated the ^{68}Ge nucleus. It turned out that the essential qualitative features of the REV results concerning the complexity of the decay pattern, the competition of various configurations corresponding to different *shapes*, etc., and even the structure of the various bands were not influenced by the additional correlations introduced by the REFV procedure. Moreover, the new ^{68}Ge data[17] are in striking agreement with the complex band structures and multiple shape coexistence predicted for ^{68}Ge, including the band-crossing transitions and the new band with superdeformation. Quantitatively, however, a number of changes were obtained, which, in particular, support the need for some modifications of the effective Hamiltonian which previously had been adjusted only within the more restricted *real* EXCITED VAMPIR approach.

Trying to confirm the complicated REFV picture for ^{68}Ge on a more quantitative basis, we have calculated the charge densities for the ground states and the transition charge densities for the first two $I^\pi=2^+$ states in several even Ge isotopes and have compared the results with the data extracted from elastic electron scattering. In the lighter nuclei ^{70,72}Ge the calculated densities are in good

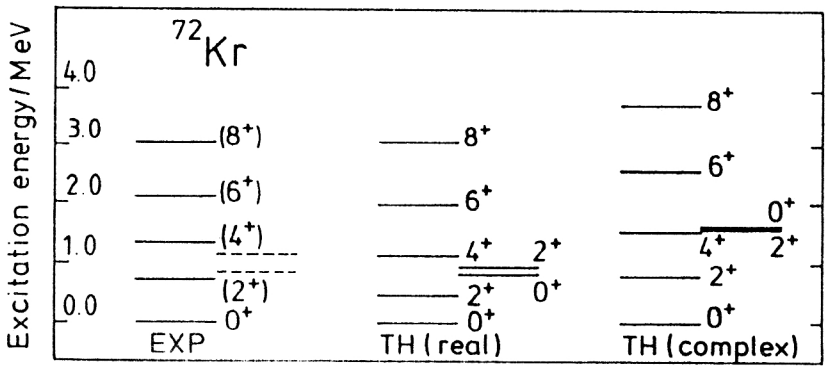

FIG. 25. The theoretical spectrum obtained within the FED VAMPIR or EXCITED FED VAMPIR approaches based on *complex* (right) and *real* (middle) HFB transformations, compared with recent experimental results[50,51] (left) for the even-spin positive-parity states of the nucleus ^{72}Kr.

agreement with experiment. In the two heavier nuclei ^{74,76}Ge, on the other hand, the calculations miss a considerable part of the collectivity observed experimentally. This defect is a strong indication that either the renormalization of the effective Hamiltonian performed up to now is not sufficient, or that, instead of the purely real HFB transformations used here, essentially complex ones should be admitted, or both. In the next section we shall introduce essentially complex HFB transformations which allow one to account for time-odd correlations in the underlying mean fields in order to learn something more about the effective two-body interaction and how it performs in a given model space.

5. COMPLEX MEAN FIELDS

The results obtained within the real VAMPIR approaches for the $A\sim 70$ mass region indicated a variable oblate–prolate mixing and a shape transition from oblate to prolate deformed shapes with increasing A. As for $N=Z$ nuclei, both neutrons and protons simultaneously fill the same levels, the neutron–proton interactions are significant, one expects that the shell stabilized shapes should be particularly bound, and a direct connection can be made between the *shape* of such a nucleus and its underlying nuclear structure. On the other hand, the description of the structure of these nuclei is a sensitive test for the theoretical models. The most sophisticated VAMPIR models going beyond mean-field approximations deal with *complex* mean fields. The use of essentially *complex* HFB transformations allows for mixing of proton and neutron basis states as well as for parity mixing, providing a possibility of accounting for time-odd unnatural-parity two-nucleon correlations, while keeping time-reversal and axial symmetry. In this section we present the picture for the shape-coexistence phenomena encountered in the $N=Z$ ^{72}Kr nucleus, emerging from the VAMPIR approaches based on *complex* mean fields. A comparison with the *real* calculations for the same model space and effective Hamiltonian is also given.

Using the "truncated" single-particle basis and the effective two-body force presented in Sec. 2.3, we constructed the *complex* EXCITED FED VAMPIR wave functions for the first two 0^+ and 2^+ states and the *complex* FED VAMPIR solutions for the yrast 4^+, 6^+, and 8^+ states in the ^{72}Kr nucleus. The linear combinations of symmetry-projected determinants constructed for a state of a given symmetry contained two to five configurations. The energy gains introduced by the additional correlating configurations to each main component were successively decreasing in any variational chain of calculations, and these were truncated as soon as the gains became of the order of 100 keV. The total energy gain brought to a state by the correlating configurations was decreasing with increasing spin, as was already found from the *real* calculations. But the same type of variational procedures applied for *real* HFB transformations in the same model space, and using the same effective force, always led to smaller energy gains from correlating configurations. A more suggestive parameter indicating the contribution of the additional correlations introduced already in the mean field by the *complex* HFB transformations is the total binding energy for the main configuration underlying the wave function of each calculated state. This supplementary energy varies between 1550 keV for the first 0^+ state and 1200 keV for the yrast 8^+ state and the first excited 0^+ state.

In Fig. 25 we compare the theoretical *complex* spectrum with the available experimental one[50,51] for the investigated states in the ^{72}Kr nucleus. The results obtained using only *real* mean fields are also plotted. One can see from this figure that the experimental behavior of the level spacing with increasing spin is well reproduced in the *complex* calculations. The main component in the wave functions for the yrast states is oblate-deformed. The additional correlations introduced by the FED VAMPIR procedure brought energy gains of 1094, 658, 602, 531, and 467 keV for the 0^+, 2^+, 4^+, 6^+, and 8^+ states, respectively. The main correlations for the 0^+ ground state came from a prolate-deformed configuration, which finally represents 34% in the wave function. The results indicate that of all the additional configurations of CFV type for these states only one is prolate-deformed. The contribution of this component in the wave function decreases with increasing spin: 7% for the 2^+, 3% for the 4^+, and less than 2% for the 6^+ and 8^+ states. The main component in the first excited 0^+ and 2^+ states is prolate-deformed. The prolate–oblate mixing appears only in the wave function for the first excited 0^+ state, where the oblate component represents 16%. Even if the nature of the main components and of the additional correlating configurations are similar to those obtained in the *complex* calculations, the trend in the level spacing of the final spectrum is different for the *real* calculations and does not reproduce the experimental one

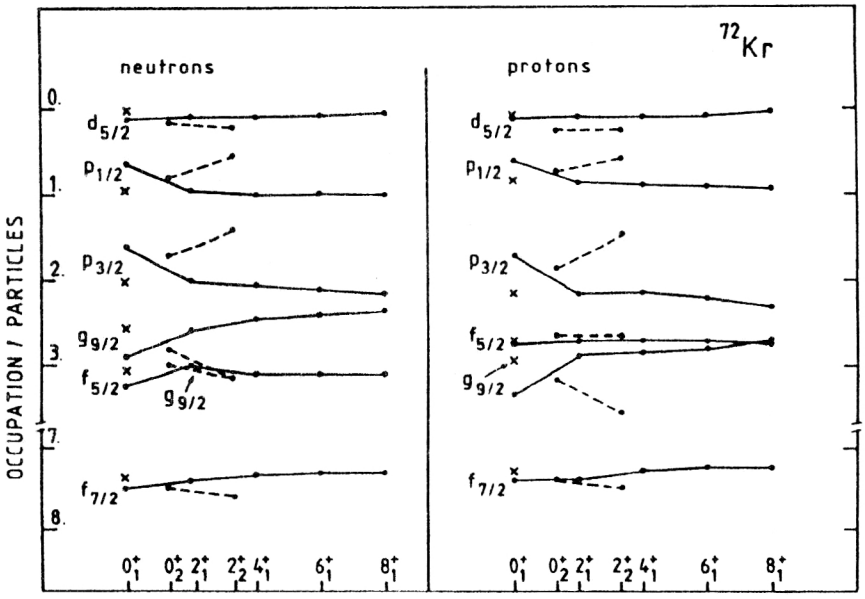

FIG. 26. Neutron and proton occupation numbers of the spherical-basis orbitals for the lowest two 0^+ and 2^+ and for the yrast 4^+, 6^+, 8^+ states in ^{72}Kr. Full lines are for yrast states, and dashed lines for the first excited states. The results have been calculated from the full wave functions, Eq. (2.24), based on *complex* HFB transformations. The crosses are for the one symmetry-projected determinant approximation to the 0^+ ground state.

equally well. The fact that the *complex* calculations reproduce the experimental trend in the level spacing is one of the improvements obtained by introducing the neutron–proton interaction and the unnatural-parity pairing correlations [see Eq. (2.19)] in the HFB vacuum [Eq. (2.18)]. This seems to be essential for the $N=Z$ ^{72}Kr nucleus.

The intrinsic quadrupole moments of the building determinants of the wave functions for all the investigated states indicate almost identical contributions coming from the neutrons and from the protons. This is a strong indication that our effective force is well chosen and adequate to describe the complex structure of the nuclei belonging to this mass region. Other results obtained from our investigations within the CFV or CEFV approximations support this conclusion. In Fig. 26 we plot the neutron and proton occupations for the spherical single-particle orbits building the model space. Again, the results indicate a very similar behavior on the neutron and proton sides. One can also observe a very smooth change with increasing spin. The 0^+ ground state has a special behavior. The crosses indicate the occupations for the main component of the corresponding wave function, which is oblate-deformed, as for the other spin states. As can be seen, it reveals occupations similar to those coming from the full wave functions for the other spin states. The strong mixing of the prolate configuration produces the deviations observed in the occupations for the final linear combination calculated for this state. The prolate–oblate mixing present only in the first excited 0^+ state but not in the 2^+-state, both containing a prolate-deformed main determinant, is also reflected by the corresponding spherical occupations. Protons and neutrons also have similar contributions, through $T=1$ like-nucleon pairing correlations, to the average pairing gap for all calculated configurations. In ^{72}Kr the contribution of the neutron–proton $T=1$ pairing correlations to the total pairing energy varies from one configuration to another: it can be negligible, comparable, and sometimes even more important than the $T=1$ like-nucleon pairing contribution. The results indicate a very small contribution from $T=0$ neutron–proton pairing correlations.

It should be mentioned that our investigations using *complex* mean fields indicate that the main configuration for the first excited 4^+ and 6^+ states in ^{72}Kr are prolate-deformed, as they appear also in the *real* calculations. Some preliminary studies of the ^{74}Kr nucleus using *complex* HFB transformations show that the main configuration for the first 0^+, 2^+, and 4^+ states is prolate-deformed.

We can conclude that the prolate–oblate shape coexistence is also found in the ^{72}Kr nucleus. A strong prolate–oblate mixing in the structure of the wave functions for a given state is obtained only for the first two 0^+ states and the yrast 2^+ state. The description of the structure of the $N=Z$ ^{72}Kr nucleus, which should mostly require the introduction of the neutron–proton interaction in the mean field, is a sensitive test for both the model and the effective force.

6. CONCLUSIONS

In the present article some recent achievements concerning the microscopic description of the shape-coexistence phenomena in the $A\sim70$ mass region have been reviewed. The theoretical models involved in these investigations were the most sophisticated approaches belonging to the VAMPIR family, based on *real* and *complex* HFB transformations. The EXCITED VAMPIR model, being essentially a mean-field approximation, and also the EXCITED FED VAMPIR method, going beyond mean fields, have been applied in a relatively large single-particle basis, using realistic effective two-body forces, particularly designed to account for the complex structure of the nuclei belonging to the $A\sim70$ region.

It was found that the shape-coexistence phenomena dominate the structure of the investigated chains of even–even Ge, Se, and Kr isotopes. The structure of these nuclei reveals both shape transition and shape coexistence. An

oblate-to-prolate shape transition with increasing A emerged from the calculations. The structure of the low-spin states in the investigated nuclei, mainly 0^+ and 2^+ states, is dominated by a strong oblate–prolate mixing. A variable mixing of more or less deformed oblate and prolate symmetry-projected quasiparticle determinants is able to produce the experimental picture for the low-spin states of the considered Ge and Se isotopes, like the presence of 4–5 coexisting 0^+ or 2^+ states in 3–4 MeV excitation energy, as well as the general trends observed for the quadrupole moments and electromagnetic transition probabilities, and proton and neutron occupations of the spherical single-particle orbitals. It turned out from the investigation of the high-spin states in some selected Ge and Se isotopes that the shape coexistence persists and manifests itself specifically at high spins. Our predictions concerning a strong bunching of states of a given medium or high spin and positive parity in a small excitation energy interval and a complex feeding pattern of the yrast line, including strong $M1$, $\Delta I=0$ transitions for medium-spin states, were confirmed by recent experimental data on the ^{68}Ge nucleus.

The recent studies concerning the structure of the $N=Z$ ^{72}Kr nucleus, based on *complex* HFB transformations, which allow one to include neutron–proton interactions and unnatural-parity pairing correlations in the mean field, revealed good agreement between the theoretical results and the available data. This is also an indication that our effective force is rather well chosen for this mass region. A slightly and carefully readjusted renormalization of the effective two-body interaction is still needed, but it requires many more experimental data than are available up to now, especially for the electromagnetic properties of the various states.

Even if a lot remains to be done, both theoretically and experimentally, the results presented here provide some interesting information on the way towards a more microscopic interpretation of the complex situation encountered in the nuclei of the $A\sim 70$ mass region.

The work presented here would have been impossible without the contribution of our collaborators: Frank Grümmer from Bochum, Esko Hammarén from Jyväskylä, Zheng Ren-Rong from Chonging, and Mauro Kyotoku from Joâo Pessoa. We are grateful to Profs. J. H. Hamilton and A. V. Ramayya for helpful discussions. One of us (A.P.) acknowledges partial support from the Internationales Büro der KfK Karlsruhe, Germany, and the University of Jyväskylä and the Ministry of Trade and Industry, Finland.

[1)]Institute for Physics and Nuclear Engineering, Bucharest, Romania.
[2)]Institut für Theoretische Physik, Universität Tübingen, D-7400 Tübingen, Germany.
[3)]Department of Physics, University of Jyväskylä, SF-40100 Jyväskylä, Finland.

[1] J. H. Hamilton, in *Treatise on Heavy-Ion Science*, edited by D. A. Bromley (Plenum, New York, 1989), Vol. 8, p. 3.
[2] M. Girod and B. Grammaticos, Phys. Rev. Lett. **40**, 361 (1978).
[3] K. Kumar, J. Phys. G **4**, 849 (1978).
[4] M. Sakakura *et al.*, Z. Phys. A **289**, 163 (1979).
[5] M. Didong *et al.*, Phys. Rev. C **14**, 163 (1976).
[6] Y. Shikata, M. Sakakura, and T. Sebe, Z. Phys. A **300**, 217 (1981).
[7] F. Sakata *et al.*, Z. Phys. A **286**, 195 (1978).
[8] K. H. Weeks, T. Tamura, and T. Udagawa, Phys. Rev. C **24**, 703 (1981).
[9] K. Takada and S. Tazaki, Nucl. Phys. **A395**, 165 (1983).
[10] A. Petrovici and A. Faessler, Nucl. Phys. **A395**, 44 (1983).
[11] A. Petrovici, A. Faessler, and T. Köppel, Z. Phys. A **314**, 227 (1983).
[12] K. W. Schmid and F. Grümmer, Rep. Prog. Phys. **50**, 731 (1987).
[13] A. Petrovici *et al.*, Nucl. Phys. **A483**, 317 (1988).
[14] A. Petrovici *et al.*, Nucl. Phys. **A504**, 277 (1989).
[15] K. W. Schmid *et al.*, Nucl. Phys. **A499**, 63 (1989).
[16] A. Petrovici *et al.*, Nucl. Phys. **A517**, 108 (1990).
[17] L. Chaturvedi *et al.*, Phys. Rev. C **43**, 2541 (1991).
[18] A. Petrovici *et al.*, Z. Phys. A **339**, 71 (1991).
[19] D. Goutte, Ph.D. Thesis, Université de Paris-Sud, Order No. ORSAY 2803 (1984).
[20] C. Bloch and A. Messiah, Nucl. Phys. **39**, 95 (1962).
[21] K. W. Schmid, F. Grümmer, and A. Faessler, Ann. Phys. (N.Y.) **180**, 1 (1987).
[22] Zheng Ren-Rong *et al.*, Nucl. Phys. **A494**, 214 (1989).
[23] A. Petrovici *et al.*, to be published.
[24] K. Holinde, K. Erkelenz, and R. Alzetta, Nucl. Phys. **A194**, 161 (1972).
[25] P. Ring and P. Schuck, *The Nuclear Many-Body Problem* (Springer-Verlag, Berlin, 1980).
[26] G. Rotbard *et al.*, Phys. Rev. C **18**, 86 (1978).
[27] G. Rotbard *et al.*, Nucl. Phys. **A401**, 41 (1983).
[28] R. Lecomte *et al.*, Phys. Rev. C **25**, 2812 (1982).
[29] S. Mordechai *et al.*, Phys. Rev. C **29**, 1699 (1984).
[30] M. Vergnes, in *Proc. of the Intern. Conf. on the Structure of Medium-Heavy Nuclei*, Rhodes, 1979 (Institute of Physics, Bristol, England, 1980), p. 25.
[31] R. Lecomte *et al.*, Phys. Rev. C **22**, 1530 (1980).
[32] A. Passoja *et al.*, Nucl. Phys. **A441**, 261 (1985).
[33] A. V. Ramayya *et al.*, Phys. Rev. C **12**, 1360 (1975).
[34] A. P. de Lima *et al.*, Phys. Rev. C **23**, 213 (1981).
[35] J. Heese *et al.*, Z. Phys. A **325**, 45 (1986).
[36] T. Mylaeus *et al.*, J. Phys. G. **15**, L135 (1989).
[37] T. Paradellis and C. A. Kalfas, Phys. Rev. C **25**, 350 (1982).
[38] C. Morand *et al.*, J. Phys. (Paris) **38**, 1319 (1977).
[39] G. M. Gusinskiĭ *et al.*, Izv. Akad. Nauk SSSR Ser. Fiz. **41**, 66 (1977); V. G. Kiptilinyi, I. Kh. Lemberg, and A. S. Mishin, in *Proc. of the Conf. on Nuclear Structure*, Riga, 1979 (USSR Academy of Sciences), p. 54.
[40] F. Christancho and K. P. Lieb, Nucl. Phys. **A486**, 353 (1988).
[41] K. Harada, Phys. Lett. **10**, 80 (1964).
[42] M. E. Barclay *et al.*, J. Phys. G **12**, 12 (1986).
[43] S. Frauendorf, Phys. Lett. **100B**, 219 (1981).
[44] P. Kemnitz *et al.*, Phys. Lett. **125B**, 119 (1983).
[45] K. P. Lieb and J. J. Kolata, Phys. Rev. C **15**, 939 (1977); H. P. Hellmeister *et al.*, Phys. Rev. C **17**, 2113 (1978).
[46] V. G. Kiptilinyi *et al.*, Bull. Acad. Sci. USSR Phys. Ser. **43**, 26 (1979).
[47] L. R. B. Elton, *Nuclear Sizes* (Oxford University Press, London, 1961); R. S. Willey, Nucl. Phys. **40**, 529 (1963).
[48] L. J. Tassie and F. C. Barker, Phys. Rev. **111**, 940 (1958).
[49] M. Girod, D. Gogny, and B. Grammaticos, in *7-ème Session d'Etude Biennale de Physique Nucleaire Aussois* (1983).
[50] B. J. Varley *et al.*, Phys. Lett. **194B**, 463 (1987).
[51] H. Dejbakhsh *et al.*, Phys. Lett. **249B**, 195 (1990).